Victor S. L'vov

Wave Turbulence Under Parametric Excitation

Applications to Magnets

With 69 Figures

Chapter 9

Springer-Verlag
Berlin Heidelberg New York
London Paris Tokyo
Hong Kong Barcelona
Budapest

9 Experimental Investigations of Parametrically Excited Magnons

9.1 Experimental Investigations of Parametric Instability of Magnons

9.1.1 Methods and Materials Investigated

As already mentioned in Chap. 5, the first experiments on the excitation of magnons by parallel pumping were carried out quite a while ago (in 1960) [9.1–3] on Yittrium Iron Garnet (YIG) which still remains one of the most popular objects used in this type of research. Today, parametric instability has been observed in a number of magnets. In addition to ferrites, these also included low-dimensional ferromagnets and antiferromagnets as well as three-dimensional antiferromagnets with various magnetic symmetries.

Research is carried out in the range of the microwave frequencies. Usually simple microwave spectrometers with direct amplification are used. Figure 9.1 (left) outlines such a setup [9.4]. The sample, oriented in a certain direction, is placed into the resonator at the antinode of the microwave magnetic field $\boldsymbol{h} \parallel \boldsymbol{H}$. The operating conditions of the generator are selected in accordance with the specific aim of the investigations. Parametric excitation of magnons was registered when the additional absorption appeared at sufficiently high microwave power. Under pulsed operation of the generator the development of the instability in time can be traced. The amplitude of the microwave magnetic field h in the sample is calculated from the magnitude of the power in the resonator and the parameters of the resonator. The threshold field h_{th} above which the parametric excitation appears is definitively related to the damping of the excited magnons $\gamma(\boldsymbol{k})$ by (4.3.21).

The calculation of $\gamma(\boldsymbol{k})$ from h_{th} is a traditional procedure in the investigations of damping. Most of the research conducted on parallel pumping is based on such traditional studies and looks for the specific mechanisms of magnon interaction with other excitations and with the inhomogeneities of the sample. The nature of the stationary state above the threshold of the parametric excitation was studied only on YIG samples and easy-plane antiferromagnets, such as $MnCO_3$, $CsMnF_3$ and $FeBO_3$. In the present chapter, we shall be concerned primarily with the experimental study of these substances. Let us first consider the measurement of constants in the spectrum of magnons $\omega(\boldsymbol{k})$ because this is of special importance for what follows.

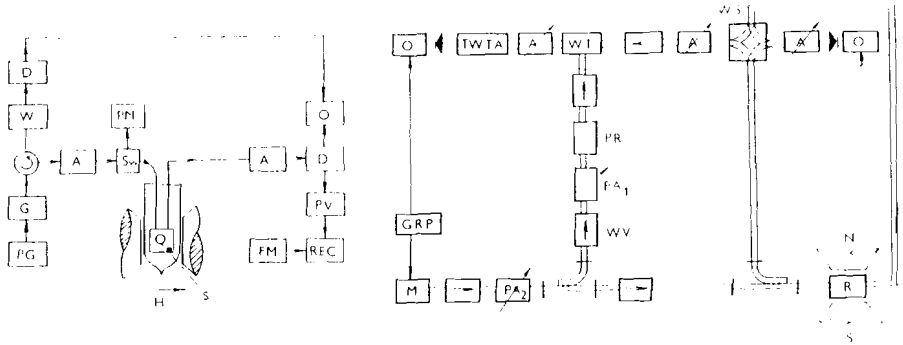

Fig. 9.1. On the left: Block diagram of the spectrometer for observing parametric excitation of magnons: G, microwave generator; A, attenuator; D, crystal detector; Sw, switch; W, wavemeter ; PM, peak-value voltmeter; FM, field meter; REC, recorder; PG, pulse generator; O, oscilloscope; S, sample (*Kotyuzhansky* and *Prozorova* [9.4]). On the right: Block diagram of the experimental setup for measuring the susceptibility χ (*Melkov* and *Krutsenko* [9.24]: M, magnetron; GRP, generator of rectangular synchronization pulses; WV, waveguide valve; WT, waveguide tee; PA, precision attenuator; PR, phase rotator; TWTA, travelling wave tube amplifier; O, oscillograph; A, attenuator; WS, waveguide switch; R, resonator

9.1.2 Measurements of Constants in Spin Wave Spectra

There exist numerous experimental methods to determine the constants of the spin wave spectrum. In order to obtain "the spectral gap", i.e. the frequency of the uniform oscillations, the electron magnetic resonance (either ferromagnetic or antiferromagnetic) is usually employed to determine the frequency. This method provides maximum accuracy. The frequencies of the inhomogeneous exchange ω_{ex} can be obtained from the temperature dependences of the specific heat and magnetization, data on inelastic neutron scattering, two-magnon light scattering, etc. We shall dwell on two kinds of experiments where these constants are obtained by using the parametric excitation of spin waves by parallel pumping.

1 Size effect This effect was discovered by *Jants* and *Schneider* and *Andlauer* in experiments on mono crystalline spheres of YIG [9.5] and afterwards it was observed by *Kotyuzhansky* and *Prozorova* on $FeBO_3$ plates [9.6]. The effect is as follows: At low damping of spin waves when their free path is longer than the sample dimensions the power passing through the resonator is not a monotonic function of H, but has dips of a resonance type under certain values of H_n. The observed phenomenon can naturally be attributed to the effect of the boundary conditions on the sample surface leading to the space resonance of the spin wave at

$$n\lambda = 2d\ . \qquad (9.1.1)$$

Here d is the dimension of the sample, $\lambda = 2\pi/k$ is the spin wave length and n is an integer. (As a rule, in these experiments $d \simeq 0.1$ cm, $k = 10^4$–10^5 and, consequently, $n \simeq 10^3$). This explanation was confirmed by the experiments on samples of different sizes. The results of one such experiment are shown in Fig. 9.2. The distance between the dips ΔH_n can be calculated from condition (9.1.1) and the formulae describing the spin wave spectra. From the comparison of the experimental and theoretical values of ΔH_n the frequency ω_{ex} can be calculated.

2 Threshold anomaly in the intersection region of spin waves and phonon spectra. The magnon and phonon branches of the energy spectra can have points of intersection. If the crystal symmetry allows the interaction of these branches, in the vicinity of these intersection points the spectra will be distorted. There are "mixed" magnetoelastic oscillations in these regions whose damping differs from the damping of magnons. Therefore h_{th} can change significantly near such intersection points. This phenomenon was first observed in monocrystals. Later, this effect was studied on easy-plane antiferromagnets (in particular, on $CsMnF_3$ and $MnCO_3$ [9.8–11]) whose spectra were intersection points at nonzero fields.

Figure 9.3.a shows such anomalies which are peak-shaped dependence of the power absorbed by the sample on magnetic field H changed. The experiments were performed by *Kotyuzhansky* and *Prozorova* [9.11] in $CsMnF_3$ at various pumping frequencies ω_p. The wave numbers at which anomalies were observed versus the spin wave frequencies are plotted in Fig. 9.3b. This dependence agrees with the dispersion law of the elementary excitation with which spin waves interact. The direct proportionality of ω and k observed in this case confirms that spin waves interact with sound waves. Using the value of the sound velocity k at the intersection point one can obtain the value of the frequency ω_{ex} in the spin wave spectrum.

9.1.3 Spin Wave Damping

The rate of damping $\gamma(\boldsymbol{k})$ with $da/dt = -\gamma a$ where a is the amplitude of the wave, is a very important characteristic of large practical significance. A detailed discussion of experimental research into the nature of relaxation is beyond the scope of our book. We shall therefore restrict ourselves to a summary of the principal relaxation processes in the magnets under study. At k not too high, far from the Brillouin zone edge, magnon damping is determined by three kinds of processes:

1 Intrinsic processes including three- and four-magnon relaxation as well as the relaxation of magnons caused by their interaction with phonons and nuclei;

2 Two-magnon processes of inelastic scattering by inhomogeneities (pores, polycrystallinity, deviations from stoichiometry, etc.);

3 "Slow" and "fast" relaxation, i.e. processes involving impurity ions with strong spin-orbit coupling.

Quite naturally we shall be interested mostly in the "eigen" relaxation because the other contributions to the damping can be substantially reduced by the selection of more perfect samples. In addition, for the investigation of the above-threshold state it is of great importance to know the dependence of the magnon damping on their number.

The simplest and most universal method for determining $\gamma(\boldsymbol{k})$ of the magnons is via calculation on the basis of the experimental values of the threshold of parametric excitation of magnons h_{th}. The absolute accuracy of this method is not high (the error is usually 20–30%) because when obtaining h_{th}, several quantities are employed which were measured with an accuracy of several per cent. These include the power input of the resonator, the coupling coefficient with the resonator, the Q factor of the resonator. In addition, the distortion of the field distribution in the resonator due to the magnetic sample cannot accurately be allowed for. However, the relative error of this method for finding the damping is only about 2%, which makes it very convenient for studying the relaxation dependence on various external parameters. Calculations are performed according to (4.3.21): $h_{\mathrm{th}}V(\boldsymbol{k}) = \gamma(\boldsymbol{k})$. The coefficient $V(\boldsymbol{k})$ in this formula depends on the kind of magnetic system being investigated and on the method of parametric excitation of magnons. The coefficients $V(\boldsymbol{k})$ for the cubic ferrimagnet and for the easy-plane antiferromagnet were given in Sect. 4.3. All the relaxation process that can occur in real experiments on these magnets have been theoretically calculated. By comparing the experimentally obtained functional dependences $\gamma(\boldsymbol{k}, H, T)$ with the theoretical prediction, the particular contributions of the specific relaxation process to the total value γ can be found. It must be noted that for YIG, $MnCO_3$, $CSMnF_3$ and $FeBO_3$ theoretical and experimental data are in fairly good agreement.

A. Yittrium Iron Garnet The most comprehensive research on relaxation in YIG was performed experimentally by *Anisimov* and *Gurevich* [9.12, 13) and theoretically (allowing for the complex magnetic structure of YIG) by *Kolokolov, L'vov* and *Cherepanov* [9.14, 15]. Figure 9.4 shows in a plot of temperature T versus wave vector k the regions where from the theoretical view-point of [9.15] the contribution of one or the other process predominates. For long spin waves $k < k_{\mathrm{e}}$ ($ak_{\mathrm{e}} \simeq 2\omega_{\mathrm{ex}}/\omega_i$) the three-magnon processes in the quasi-ferromagnetic branch of the spectrum are forbidden by the conservation laws, and the amplitude of the exchange four-magnon processes is very small. The damping $\gamma(\boldsymbol{k})$ under $k \to 0$ was first experimentally studied by *Kasuya* and *Le Craw* [9.16] who assumed that the damp-

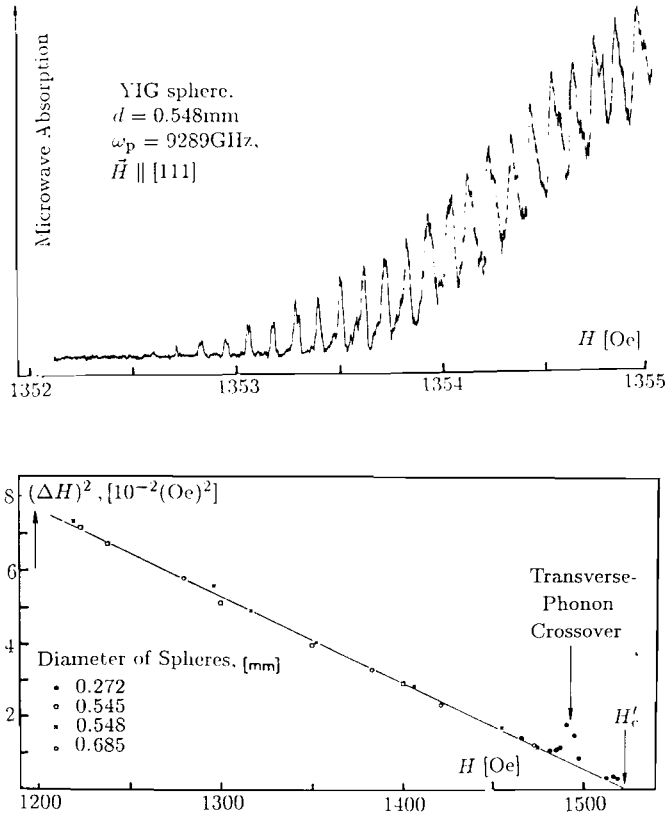

Fig. 9.2. (a) Absorbed microwave power versus magnetic field upon excitation of spin waves by parallel pumping in a YIG sphere (*Jantz* et al. [9.5]). (b) Intervals ΔH between absorption peaks versus magnetic field. Results obtained for four spheres of different diameters d, normalized to $d = 0.3$ mm

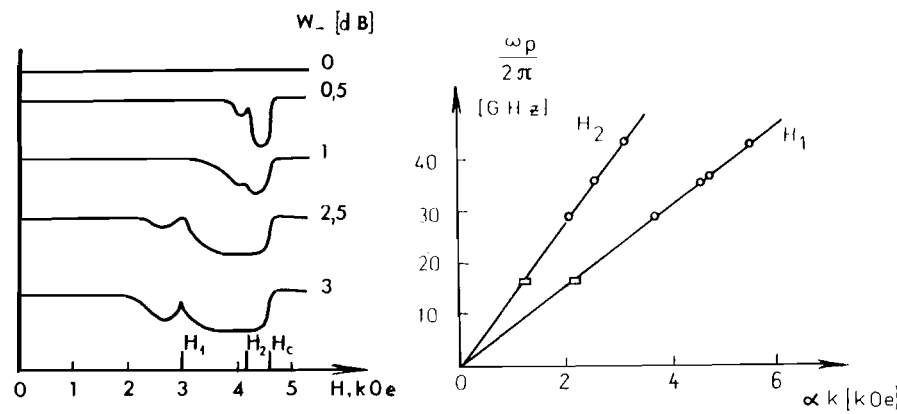

Fig. 9.3. (a) Absorbed microwave power versus magnetic field upon excitation of spin waves by parallel pumping in a YIG sphere. (b) Intervals ΔH between absorption peaks versus magnetic field. Results obtained for four spheres of different diameters d, normalized to $d = 0.3$ mm (*Jantz* et al. [9.5])

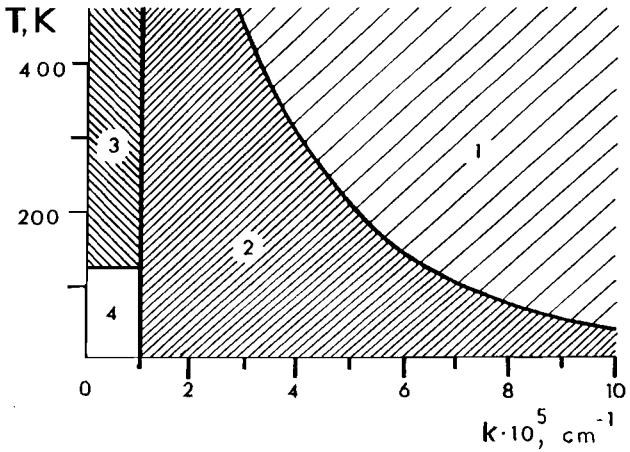

Fig. 9.4. Diagram of the relative contribution of various relaxation processes in YIG. Numbers indicate the region in which the various relaxation processes predominate: (1), four-magnon; (2), three-magnon with the participation only of magnons of the quasi-ferromagnetic branch of the spectrum; (3), with the participation of optical magnons; (4), scattering by defects. Calculated for $\omega_k/2\pi$ =4.7 GHz (*Kolokolov* et al. [9.15])

ing was caused by the three-particle process involving an optical magnon and a phonon. In [9.15] such processes have been analyzed in detail and it was shown that the main contribution to the damping of magnons with $k \to 0$ was made by the process of confluence of the ferromagnon and optical magnons. The amplitude of this process is proportional to the energy of a uniaxial crystallographic anisotropy of ions Fe^{3+} in the octahedral sites. At low temperatures $T < 120$ K the damping $\gamma(0)$ exponentially decreases. In this temperature range (range 4) the main eigen process of relaxation is the four-magnon magneto-dipole scattering. However, under real conditions at $T < 120$ K and $k < k_e$ the damping of ferromagnons is as a rule due to the defects [9.17]. In the range (2) the magneto-dipole three-magnon relaxation prevails which is determined by two processes, i.e. confluence and decay

$$\omega(\boldsymbol{k}) + \omega(\boldsymbol{k}') = \omega(\boldsymbol{k} + \boldsymbol{k}'), \quad \omega(\boldsymbol{k}) = \omega(\boldsymbol{k}') + \omega(\boldsymbol{k} - \boldsymbol{k}') \,. \tag{9.1.2,3}$$

The decay processes are allowed at $k > k_S$. The quantity k_S is given by

$$\omega(k_S) = 2\omega(k_S/2) \,. \tag{9.1.4}$$

Both in confluence and decay processes $\gamma(\boldsymbol{k}) \propto T$, but the dependence γ of k differs for these processes. Experimentally, at $k = k_S$ a characteristic point is observed in the experimental γ–versus–k curve. In the range (1) the four-magnon exchange scattering is the main process and

$$\begin{aligned}\gamma(\boldsymbol{k}) =& \text{const} \cdot \omega(\boldsymbol{k})(ak)^2 \left(\frac{T}{\omega_{ex}}\right)^2 \left[\ln^2\left(\frac{T}{\omega(\boldsymbol{k})}\right)\right. \\ & \left. - 3.3\ln\left(\frac{T}{\omega(\boldsymbol{k})}\right) - 0.3\right] \text{ at } T < 200 \text{ K} \,, \\ \gamma(\boldsymbol{k}) =& \text{const } T\omega(k)(ask)^2 (T/\omega_{ex})^4 \text{ at } 350 \text{ K} > T > 200 \text{ K}\end{aligned} \tag{9.1.5}$$

At room temperature in YIG $\gamma(0) = 2.4 \cdot 10^6$ s^{-1}, $\gamma(k)$ is the k-dependent part of the damping γ being of the same order of magnitude at $k \simeq 10^5$ cm.

B Antiferromagnets with anisotropy of the "easy-plane" type: $MnCO_3$ and $CsMnF_3$. Relaxation of magnons in these antiferromagnets was investigated within the temperature range 1.2–4.2 K and in the frequency range $\omega(\boldsymbol{k})$ from 10 to 20 Hz [9.8–12]. It was shown that under these conditions $\gamma(\boldsymbol{k})$ varies from 0.1 to 10 MHz. For the relaxation of magnon at liquid helium temperatures the following facts are essential: (i) The presence of a low-frequency quasi-ferromagnet branch of the spectrum ($\omega_2(0)/2\pi \simeq 10^{11}$ Hz); (ii) The velocities of magnons and phonons are close; (iii) There is strong hyperfine interaction in antiferromagnets with Mn^{2+} ions. According to theory the following processes of relaxation are important:

1. confluence of two magnons of the quasiferromagnetic branch into a magnon of the quasiferromagnetic branch γ_{3m},
2. magnon-phonon interaction $\gamma_{m,ph}$,
3. magnon scattering on the paramagnetic subsystem of ^{55}Mn nuclei-γ_{mn}.

The relaxation parameters γ_{3m}, $\gamma_{m,ph}$ and γ_{mn}, have different functional dependences, and therefore the contributions of each mechanism can be separated. The first process is basic at comparatively high temperatures and strong magnetic fields $\gamma_{3m} \propto H^3 \exp T$. The quality γ_{3m} coincides with the theoretical value γ_{3m} calculated by *Sobolev* and given in [9.19]. For the second process *Lutovinov* obtained $\gamma_{m,ph} \sim T\Theta^2$ [9.19] (where Θ is the constant of the magnetoelastic interaction). As the temperature decreases the process of magnon scattering on magnetization fluctuations of the nuclear subsystems becomes predominant. As follows from theoretical research by *Woolsey* and *White* $\gamma_{mn} \sim AI(I+1)k/\omega_p$ [9.21], (where A denotes the constant of the hyperfine interaction, I is the spin of the nucleus), in all the investigated substances the experimental value of γ_{mn} is in good agreement with the theoretical result [9.21]. Therefore all these processes in combination enable us to describe the relaxation at helium temperatures in the antiferromagnets $MnCO_3$ and $CsMnF_3$.

$FeBO_3$: The magnon damping was studied in a wider temperature range, i.e. from 1.2 to 150 K [9.18] (The measurements were taken at the pumping frequency $\omega_p/2\pi = 36$ GHz, γ was changed within the range 1 –50 MHz). Unfortunately it was not possible in this case to avoid the "slow relaxation"

caused by the presence of Fe^{2+} ions which results in maximum at $T \simeq 18$ K. At higher temperatures, the damping is determined by three-magnon processes, at lower temperatures it is mainly influenced by the magnon-phonon processes. The energy spectrum qualitatively differs from the $MnCO_3$ and $CsMnF_3$ spectra – the magnon and phonon branches do not intersect, because the limiting "magnon velocity" $a\omega_{ex} > u$ (u is the sound velocity). In this connection, in addition to the process of confluence involving the phonons in the region of fields where the group velocity of magnons is lower than the sound velocity, the process of decay into a magnon and phonon is also allowed.

9.2 Nonlinear Behavior of Parametric Magnons – General Information

9.2.1 Measuring Technique for Susceptibilities χ' and χ''

A traditional method for investigating the above-threshold state of magnons is to measure the high-frequency susceptibility $\chi = \chi' + i\chi''$ above the parametric excitation of magnons. These values are connected by (5.5.31) with the distribution function $\sigma(\boldsymbol{k})$. It is possible to say that the value χ is determined by the total number of parametric waves N and by its phase Ψ. The shape of χ' and χ'' dependences on the pumping intensity significantly depends on the mechanism of amplitude limitation (see (5.5.34, 35)). In traditional experimental measurements of the magnetic susceptibility the reaction of a high-quality resonator to the changed state of the sample inside it is usually employed. The resulting quality change of the resonator determines the imaginary part of the susceptibility χ'', and the change in the eigenfrequency determines the real part of χ'. The measuring technique of the nonlinear susceptibilities under parallel pumping differs from the standard measuring techniques in some specific features, i.e. pulsed operation of the microwave generator, wide field range where the energy absorption is observed, χ' and χ'' dependence on the pumping intensity. The latter leads to the fact that the power of the generator is not a good measure of the pumping field amplitude. The field h in the resonance is more conveniently determined from the output power of the resonator. This enables one to automatically allow for the feedback effect of spin waves on the pumping which is substantial near the threshold even if the filling factor of the resonator is small.

The typical experimental setup for the study of parallel pumping is shown in Fig. 9.1 (on the left) [9.22]. The principle of its operation is as follows. The excitation of spin waves deteriorates the loading quality of the resonator Q and its eigenfrequency ω_0 is changed, which brings about the echo signal informing us about the values of χ' and χ''. The quantity χ''

is connected with the reflection coefficient Γ in the exact resonance (at $\omega = \omega_0$) by the following relation [9.23]

$$\chi'' = AQ_H\Gamma/(1-\Gamma)\,, \tag{9.2.1}$$

where $A = 2\pi \int_{VS} h^2 d\boldsymbol{r} / \int_{VC} h^2 d\boldsymbol{r}$ is the filling factor of the resonator equal to the ratio of the integrals over the sample volume VS and resonator volume VC. The real part of the susceptibility χ' is directly determined by the frequency shift $\Delta\omega = \omega_{res} - \omega_{res,0}$ where $\omega_{res,0}$ is the eigenfrequency of the empty resonator and ω_{res} is the eigenfrequency of the resonator-sample system. These frequencies correspond to the minimum of the reflection coefficients (for the empty resonator and for resonator, wich contains a sample). For several reasons, mainly because of the inaccurately determined coefficient A, the measuring error of absolute values χ' and χ'' is usually of the order of 20–40 %. All this has result in a wide spread of experimental data of different researchers and no unambiguous interpretation of the nature of the above-threshold state has been put forward.

Melkov and *Krutsenko* in their research of the above-threshold state in YIG [9.24] significantly improved the measuring technique and the measuring error was reduced to several per cent. The block diagram of the experimental setup is shown in Fig. 9.1 (on the right). The amplitude and phase of oscillations in the resonator are measured by comparing the signal that had passed through it with the reference signal. When the pumping amplitude is below the threshold value ($h < h_{th}$) the signal is compensated to zero. When $h > h_{th}$ it results in the magnetization in the sample $m_z(\omega_p) = \chi h(\omega_p)$ changing with the pumping frequency and directed along $\boldsymbol{H}$. The magnetization m_z brings about the additional microwave magnetic field in resonator $h_p(m_z)$. It causes the changes in the amplitude and phase of the total self-consistent magnetic field of the resonator with respect to the amplitude and the phase of the pumping. These changes can be measured by a phase rotator PR and amplitude attenuator PA placed in the reference signal channel by the compensation of the mismatch signal due to the parametric excitation of magnons. Evidently, if the change in the amplitude $a = h/h_{th}$ and in the field phase ψ in the resonator are known, information about the microwave magnetic field of reaction $h_p(m_z)$ and, consequently, about the nonlinear susceptibility can be obtained

$$\chi' = -4\pi\omega_p^2 aA\sin\psi\,,\quad \chi'' = 4\pi\omega_p^2 aA\sin\psi[\mathrm{ctg}\psi - (\sin\psi)/a]\,. \tag{9.2.2}$$

Clearly, from χ the phase of the pair Ψ can be calculated since $\mathrm{tg}\Psi = \chi''/\chi'$. Measurements were usually carried out at $\omega_p/2\pi = 9.37$ GHz during the pulsed operation (pulse duration was 200 ms, the pulse repetition frequency was equal to 50 Hz). Spherical YIG samples with a diameter from 1 to 4 mm were mostly employed. The characteristic orientations of the magnetic field $\boldsymbol{H}$ are [100], [111] and [110].

9.2.2 Comparison of the S-Theory and Experiment for Susceptibilities

With such a comparison for cubic ferromagnets in view, let us represent (5.5.13) for χ in the following form (allowing for the axial symmetry by means of the invariant phase (5.5.8)):

$$\chi' = \frac{2}{h}\int_{-1}^{1} V(x)n(x)\cos\Psi_{\rm inv}(x)dx$$
$$= \frac{2}{h^2}\int_{-1}^{1} S_{\rm inv}(x,x_1)n(x)n(x_1)\cos[\Psi_{\rm inv}(x)-\Psi_{\rm inv}(x_1)]dxdx_1\ , \quad (9.2.3)$$
$$\chi'' = \frac{2}{h}\int_{-1}^{1} V(x)n(x)\sin\Psi_{\rm inv}(x)dx = \frac{2}{h^2}\int_{-1}^{1}\gamma(x)n(x)dx\ .$$

Clearly, the imaginary part of the susceptibility χ'' characterizes only the total number of parametric waves, at the same time the real part of χ' significantly depends on the phase relations between the pairs. Therefore, the quantity χ' is a finer characteristic of the system sensible to the details of the pair distribution in space, to auto-oscillations, inhomogeneities, etc. This can account for the considerable divergences in experimental values of χ' in different publications. Thus, for instance, in one of the earlier works by *Hartwick* et al. [9.25] it was reported that in YIG the relation $\chi'/\chi'' = 0.1$ and that depends only weakly on the magnetic field. Because of the smallness of this relation,different kinds of nonlinear damping leading to $\chi' = 0$ were suggested as the limiting mechanism (*Schlömann* [9.27]). The description of the behavior of spin waves above the threshold of parametric excitation given by *Monosov* in [9.28] and in particular the mechanism of the amplitude "self-suppression" was also essentially based on the assumption that $\chi' \ll \chi''$. However, subsequent careful investigation of the behavior of χ' and χ'' in different experimental situation showed that in perfect monocrystals in the absence of auto-oscillations the value χ' is not small and can even exceed the value of χ''.

Figure 9.5 shows the characteristic dependences of $\chi'(h^2)$ and $\chi''(h^2)$ for a YIG sphere in three basic crystallographic directions, i.e. in the direction [100] when there are no magnetization oscillations and in the directions [111] and [110] when intense auto-oscillations are observed. One can see, first, that the auto-oscillations of the magnetization does not significantly affect the value of χ'' and, second, that AOs reduce χ' to a fraction of its value. This can be explained by the fact that high above the instability threshold

$$\sin\Psi = h_{\rm th}/h \ll 1\ , \quad |\cos\Psi| \simeq 1-(1/2)(h_{\rm th}/h)^2\ , \quad (9.2.4)$$

i.e. the cosine of the phase shift of pairs with respect to the pumping which determines the value χ' is close to its extremum. Thus the auto-oscillations

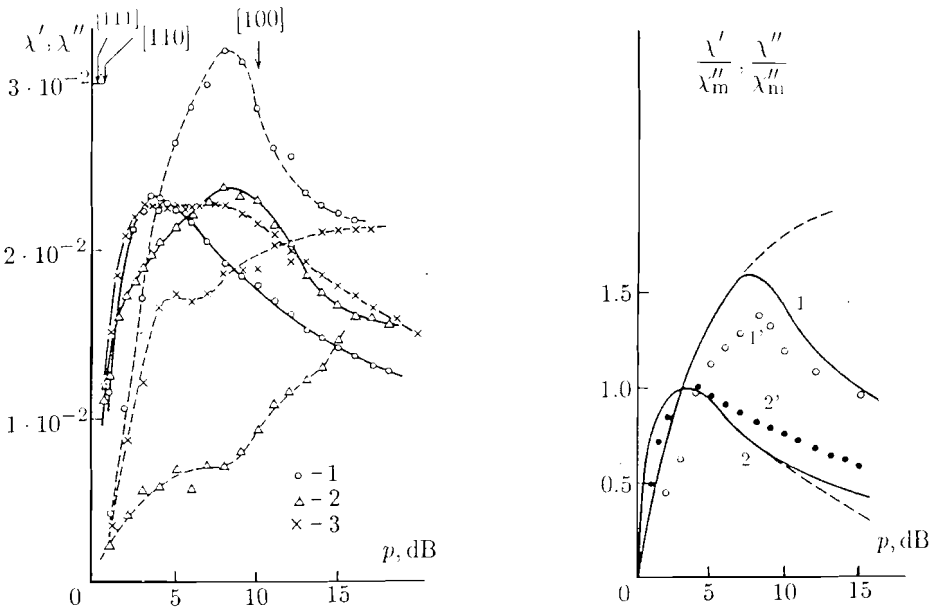

Fig. 9.5. (left) Experimental dependences of the real part of nonlinear susceptibility χ' (dashed lines) and the imaginary part of nonlinear susceptibility χ'' (solid lines) on the pumping power for a YIG sphere in three basic crystallographic directions: (1) – direction [100]; (2) – [111]; (3) – [110]. Arrows denote the thresholds of auto-oscillation excitation (*Zautkin* et al. [9.22])

Fig. 9.6. (right) Real part of nonlinear susceptibility χ' (1, 1') and imaginary part χ'' (2, 2') versus pumping power for a YIG sphere at $H = H_c - 100$ Oe, $\boldsymbol{M} \parallel [100]$. The calculation results are shown by solid lines; dashed lines correspond to the calculations in the model of one group of pairs; dots denote experimental results (*Zautkin* et al.[9.22])

(which lead to the periodical changes of the angle Ψ) do not change the mean value of $\sin\Psi$, and reduce the mean value of the $\cos\Psi$ together with the susceptibility χ'.

The fact that $\chi' \simeq \chi''$ is an unambiguous evidence of the significant phase mismatch of the pumping and magnon pairs which was predicted by the S-theory. The comparison of its prediction with the experimental dependences $\chi'(h)$ and $\chi''(h)$ is significantly facilitated under small supercriticality ($h < h_2$) when only the pairs on the equator with $\Theta = \pi/2$ are excited. In this case it follows from (9.2.3) and (5.5.12) that

$$\chi'' = \frac{2V_1^2}{|S_{11}|}\frac{h_{\rm th}\sqrt{h^2-h_{\rm th}^2}}{h^2}\ , \quad \chi'' = \frac{2V_1^2}{S_{11}}\frac{(h^2-h_{\rm th}^2)}{h^2}\ . \quad (9.2.5)$$

Fig. 9.6. shows the qualitative agreement between the theoretical and experimental curves (see Fig. 9.5 for $\boldsymbol{M} \parallel [100]$). For example, according to the theory the curve $\chi'(h)$ intersects the curve $\chi''(h)$ at the maximum. The discrepancy between the theoretical and experimental curves $\chi'(h)$ at $h > 8$ dB

can be naturally explained by the excitation of the second group of pairs which do not allow for (9.2.5).

Computer calculations aimed at the comparison of the S-theory with the experimental data were performed by *Zautkin* et al. [9.22]. To this end, first the functions $S(x,x')$ were calculated by (3.1.21) under specific experimental conditions for YIG, i.e. magnetization, field of the crystallographic anisotropy and exchange field. The obtained values were substituted into the nonstationary equations of motion of the S-theory (5.4.13) which were solved on computer by time iteration with respect to the level of the thermal noise. The obtained stationary values of the amplitudes and phases under different supercriticalities made it possible to calculate the values of χ' and χ'' by (9.2.3). The calculation results are shown in Fig. 9.6 as well as the results of the laboratory experiment. Not only qualitative but also good quantitative agreement of theoretical and experimental results is evident.

Table 9.1. Comparison of the theoretical and experimental values of nonlinear susceptibility $\chi''_{\rm m} = \max_h \chi''(h)$ for spherical samples of different crystals: (1) $Y_3Fe_5O_{12}$; (2) $Y_3Fe_{4.35}O_{12}$; (3) $Bi_{0.2}Ca_{2.8}Fe_{3.6}V_{1.4}O_{12}$; (4) $Li_{0.5}Fe_{2.5}O_4$; (5) $NiFe_2O_4$. (After *Zautkin* et al. [9.22])

Crystal	$4\pi M$ [Oe]	H_a [Oe]	$2\Delta H(k)$ [Oe]	$\chi''_{\rm m}$ Exper.	$\chi''_{\rm m}$ Theory	Direction
1.	1750	84	0.12	24	21	[100]
2.	1500	8	0.36	23	22	[100]
3.	650	58	0.45	5.0	7.5	[100]
4.	3700	580	0.80	80	70	[111]
5.	3200	490	1.40	25	19	[100]
5.	—	—	—	55	84	[111]

Table 9.1 shows the comparison of the theoretical and experimental values of the maximum susceptibility $\chi'' = \max \chi''(h)$ for various spherically shaped cubic ferromagnets. Absolute susceptibility measurements were performed for YIG by using the standard technique described in the previous section. The values χ'' for other crystals were measured on the same setup comparing it to YIG. The theoretical values were calculated by (9.2.5)

$$\chi''_{\rm m} = V_1^2/|S_{11}| \,, \tag{9.2.6}$$

which for cubic ferromagnets in the case of axial symmetry $\boldsymbol{M} \parallel [111], [100])$ after the expressions for V and S are substituted assumes the following form (*Zautkin* et al. [9.22]):

$$8\pi\chi''_{\rm m} = [N_z - 1 + \delta(\omega_a/\omega_{\rm m}) + \sqrt{1 + (\omega_{\rm p}/\omega_{\rm m})^2}]^{-1} \,, \tag{9.2.7}$$

where δ is given by Table 3.1.

As can be seen from Table 9.1 the simple formula (9.2.7) gives a good description of the absolute values of the above-threshold susceptibility for a wide class of cubic ferromagnets. A certain discrepancy between theory and experiment for $NiFe_2O_4$ (orientation [111]) is evidently due to the fact that in this case the susceptibility maximum is above the generation threshold of the second group of pairs when (9.2.7) cannot be applied.

Green and *Healy* [9.29] measured the susceptibility $\chi''_{\rm m}$ for the uniaxial ferromagnet $Ba_2Zn_2Fe_{12}O_{14}$ with easy-plane anisotropy and obtained an abnormally high value of $\chi''_m \simeq 0.2$. The theoretical estimation of χ''_m from (9.2.6) with the coefficients V_1 and S_{11} and calculated not allowing for the dipole-dipole interaction (at $\omega_{\rm m} < \omega_a$, $\omega_{\rm p} \le \omega_a$) is

$$2\pi\chi''_{\rm m} = \omega_{\rm m}\omega_a/\omega_{\rm p}^2 \,.$$

Taking from [9.29] the parameter values for $Ba_2Zn_2Fe_{12}O_{14}$, $4\pi M = 2850$ Oe, $\omega_a/g = 9900$ Oe and the pumping frequency $\omega_{\rm p}/g = 6300$ Oe we obtain $\chi''_{\rm m} \simeq 0.1$. There is a qualitative agreement between the theoretical and experimental values of χ'' also under the parametric excitation of magnons in antiferromagnets (*L'vov* and *Shirokov* [9.30]; *Prozorova* and *Smirnov* [9.31]).

It is rather interesting to compare theory and experiment for the signs of the real susceptibility χ'. According to (5.5.35) the signs of the of χ' and S coincide for cubic ferromagnets. In accordance with the theoretical predictions $\chi' > 0$ for the weakly anisotropic crystal (enumerated in Table 9.1. as $1,2,3$) and $\chi' > 0$ for crystals with high anisotropy (number $4,5$) for orientation [100] and $\chi' < 0$ for orientation [111].

9.2.3 Measurements of Interaction (Frequency Shift) Amplitude

If $n(\boldsymbol{k},t)$ rapidly changes with the development of the parametric instability, then the eigenfrequency of magnons and the pumping frequency become mismatched. This is revealed also when the pulse after passing through the resonator is somewhat distorted. However, frequency renormalization in such an experiment cannot be studied with sufficient accuracy since as the instability develops, the microwave field amplitude and magnon damping change. *Prozorova* and *Smirnov* [9.31] employed the following method for the measurements of the nonlinear magnon frequency shift $\omega_{\rm NL}(\boldsymbol{k}_1,t)$ under a drastic change in the number of other magnons with the frequency $\omega_{\rm NL}(\boldsymbol{k}_2,t)$. Two pumping signals with the frequencies $\omega_{\rm p1} = 2\omega(\boldsymbol{k}_1)$ and $\omega_{\rm p2} = \omega(\boldsymbol{k}_2)$ (parametrically exciting magnons with different frequencies) were applied to the crystal under investigation. The sample was placed into a rectangular resonator containing a copper strip. The dimensions of the resonator were chosen so that the frequency TE_{021} of the volume mode of the resonator should correspond to $\omega_{\rm p2}$ and the frequency of the eigen mode of the band resonator should correspond to a lower frequency $\omega_{\rm p1}$.

The crystal was placed in the antinode of both high frequency magnetic fields and was set up to satisfy parallel pumping conditions. The use of the microwave filters facilitated the separate reception of signals. The measurements were performed on the $CsMnF_3$ monocrystals at $T = 1.62$ K at the frequencies $\omega_{p1}/2\pi = 21.36$ GHz and $\omega_{p2}/2\pi = 35.1$ GHz in the magnetic fields allowing parametric excitation of magnons at both frequencies.

Figure 9.7 shows the oscillograms of the microwave pulses that had passed through the resonator. The upper beam corresponds to the signal with the frequency ω_{p1}, and the lower beam to the signal with the frequencies ω_{p2}. One can see in the upper pulse two transient processes. The first one is usual transient processes when the microwave power with frequency is ω_{p1} switched on. The second one corresponds to the time of an avalanche-type increase of the amplitude of magnons with the frequency $\omega(\boldsymbol{k}_2)$. This can be interpreted as the transition of the system of PM1 excited by the pumping with the frequency ω_{p1} into a new stationary state associated with the renormalization of the frequency $\omega_{NL}(\boldsymbol{k}_1)$ because of the amplitude increase of PM2. In the stationary state the following conditions

$$\partial\Psi(k_1,t)/\partial t = 0\ , \quad \partial n(k_1,t)/\partial t = 0$$

and relation (5.5.12) must be satisfied. If (5.5.12) is violated, the phase $\Psi(\boldsymbol{k}_1)$ deviates from its stationary value and, according to (5.3.4) the energy flux W into the sample changes, which shows in the pulse passed through the resonator.

The nonlinear frequency shift was measured using the fact that the similar transient process must be observed at the pulse with the frequency ω_{p1} when the pumping frequency discontinuously changes by amount

$$\delta\omega_{p1} = -2\Delta\ , \tag{9.2.8}$$

because in this case the relation (5.5.12) is also violated. In order to change ω_{p1} an additional rectangular pulse with variable slope of its front edges was fed to the repeller plate of the corresponding klystron. Setting the time of the pumping frequency change equal to the time of the avalanche development and the magnon lifetime, respectively, and selecting $\delta\omega_{p1}$ such that the transient processes should be completely identical, we can obtain the frequency shift Δ from (9.2.8). The quantity Δ was found to be proportional to the number of PM2. After that, the coefficient $T(\boldsymbol{k}_1,\boldsymbol{k}_2,H)$ was calculated (for the $CsMnF_3$ sample with the volume of 1 cm in the field of 1.1 kOe, $T(\boldsymbol{k}_1,\boldsymbol{k}_2,H)/2\pi \simeq 3\cdot 10^{-12}$ Hz). The quantity $n(\boldsymbol{k}_1)$ was used in calculations, obtained from (5.5.12). Theoretically, the dependence $T(\boldsymbol{k}_1,\boldsymbol{k}_2,H)$ for the antiferromagnets of the "easy-plane" type was calculated by *L'vov* and *Shirokov* [9.30]. Within the experimental accuracy there is an agreement of the theoretical and experimental results.

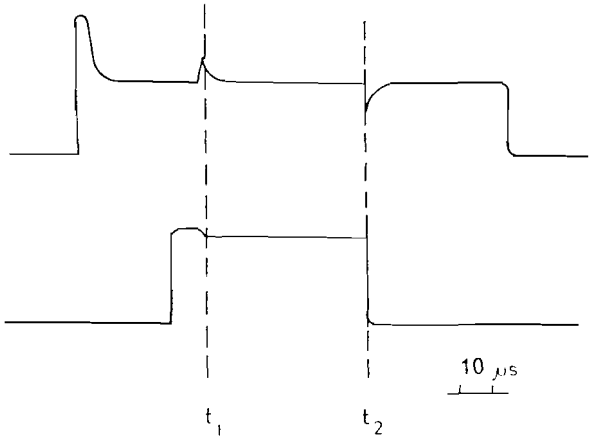

Fig. 9.7. Oscillogram of pulses after passing through the resonator. The lower beam ($\omega_p/2\pi = 35.1$ GHz) corresponds to the excitation of PM1, which causes a shift of the magnon's spectrum; the upper beam ($\omega_p/2\pi = 21.36$ GHz) corresponds to the excitation of PM2, which detects this shift (*Prozorova* and *Smirnov* [9.31])

9.2.4 Nonlinear Ferromagnetic Resonance

In this section the nonlinear theory of the ferromagnetic resonance by *L'vov* and *Starobinets* [9.32] is compared with experiments [9.33]. Unlike the early theory of *Suhl* [9.34] taking into account the interaction of only one uniform precession with parametric magnons, the nonlinear theory [9.32] allows also for the interaction of parametric magnons with each other within the scope of the basic S-theory (see Sec. 6.3). In the experiments of *Gurevich* and *Starobinets* [9.33] under the second-order instability the amplitude in the uniform precession above the threshold drastically increases which can be interpreted as the qualitative confirmation of the mechanism of magnon–magnon interaction. The shape of the resonance curve under large p is usually much more complex than shown in Fig. 6.6. There are dips on the curve and at some detunings some auto-oscillations are observed. In our opinion, they are due to the loss of stability. This is confirmed by the numeric experiment on nonlinear equations (6.3.3) describing the nonlinear ferromagnetic resonance performed by *Zakaidaikov* and *Musher*. The auto-oscillations have been treated in detail in Chap. 7 for a simpler situation, i.e. parallel pumping of magnons in cubic ferromagnets.

Let us compare the obtained results with the measurements by *Gurevich* and *Starobinets* [9.32], who measured the nonlinear susceptibilities χ' and χ'' depending on the amplitude of the pumping p under the first-order instability when the uniform precession is not at resonance $\delta \gg 1$ (see Fig. 9.8). This figure shows the theoretical dependences calculated by (6.3.21, 23), and the parameter d entering into the equations of the theory was obtained from the conditions of equality of the experimental and theoretical

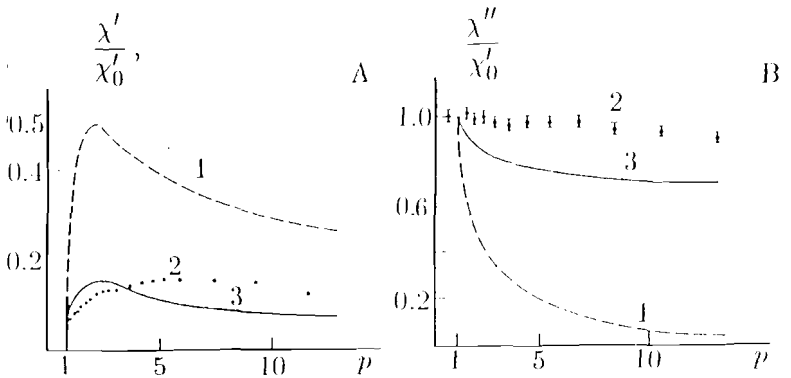

Fig. 9.8. Comparison of theoretical and experimental dependences of nonlinear susceptibilities χ'' (A) and χ' (B) on pumping power under Shul's first order instability: (1) *Shul* theory [9.34], (2) experiment [9.32], (3) *L'vov – Starobinets* theory at $d = 3 \cdot 10^{-4}$

values of $\chi''_{\max}$. It turned out that $d \simeq 3 \cdot 10^{-4}$. This order of magnitude is in good agreement with the theoretical results (see (6.3.22)). In spite of the smallness of the value, to take it into account (i.e. allowing for magnon–magnon interaction) significantly influences the form of the dependences $\chi'(p)$, $\chi''(p)$. Fig. 9.8 for comparison shows the theoretical dependences for the case $d = 0$, corresponding to *Suhl* [9.34].

9.3 Investigations of Stationary State With One Group of Pairs

From the viewpoint of the detailed comparison of the basic S-theory with the experiment the state with one group of similar pairs is undoubtedly of greater interest. First, because this mode serves as an illustrative example of a high-degree self-ordering of the flux equilibrium in the system with a large number of degrees of freedom. Second, because the distribution function of pairs is so simple that it is easily to find simple analytical expressions for the values which can be experimentally measured. The possibility of unambiguous interpretation provides the basis for consistent and detailed experimental study of the behavior of the nonlinear system of interacting parametric magnons. Such research has been carried out mostly in the former USSR by *Starobinets, Melkov, Prozorova, Ozhogin, Smirnov, Zautkin* and their colleagues. Some of these experiments are described in this chapter. We shall begin with a more detailed discussion of the nonlinear susceptibility of χ in the state with one group of pairs.

9.3.1 Nonlinear Susceptibility in the One-Group State

In Sec. 9.2.2 it was shown that the numerical values of susceptibilities agree with the formulae of the basic S-theory and that there is a qualitative agreement of theory and experiment for χ' and χ'' dependence on the pumping intensity. For the quantitative comparison of the χ'' dependence on $p = h^2/h_{\text{th}}^2$ it is convenient to represent the experimental data as the dependence of $f = \chi'' p$ on $\chi = (p-1)$ because in the S-theory this dependence (9.2.5) is the power function

$$f = \chi'' p = \chi''_{\text{m}} \sqrt{p-1} \,. \tag{9.3.1}$$

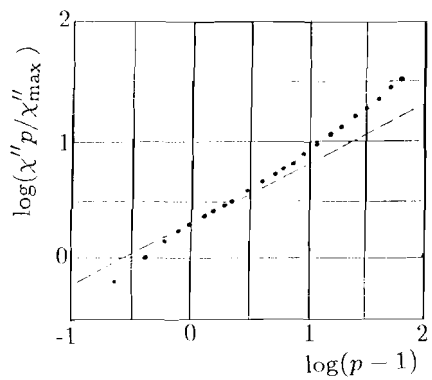

Fig. 9.9. Comparison of theory (dashed line) and experiment (dots) for absorbed power $W \propto p\chi''/\chi''_{\max}$ versus supercriticality $(p-1)$ (in the log-log plot), YIG sphere, $H_c - H = 100$ Oe, $\boldsymbol{M} \parallel [100]$. After *Zautkin* et al. [9.35]

For a detailed comparison of the theory with the experiment *Zautkin* et al. [9.35] represented (see Fig. 9.9) the experimental data for YIG (at $\boldsymbol{M} \parallel [100]$ when intense auto-oscillations are absent. The value of the magnetic field H was selected equal to $H_c - 100$ Oe, so that the nonlinear damping in the "rectifying" logarithmical coordinates is insignificant. The linear dependence obtained by them implies that

$$f_{\text{exp}} = p\chi'' = C(p-1)^z \,. \tag{9.3.2}$$

At the same time the constant C characterizing the numerical value of the susceptibility, as it was shown in Sec. 9.2.2, practically coincides with its theoretical value. Therefore we can say that there is complete agreement of the experiment with the theory (9.3.1) if we neglect a certain difference in the exponent of z (tangents of the straight lines slope in Fig. 9.9). A small divergence $z_{\text{exp}} = 0.7$ and $z_{\text{theor}} = 0.5$ is not too surprising if we take into consideration that the basic S-theory assumes that the medium is ideally homogeneous and real crystals contain some inhomogeneities, impurities, etc. Two magnon elastic scattering (on inhomogeneities, etc.) weaken the rigid phase correlations in the pairs. This results in some weakening of the phase mechanism of their amplitude limitation and, consequently, faster

increase ($z > 0.5$) of the absorbed power as the power of the pumping level increases.

9.3.2 Direct Measurement of Pair Phase

Prozorova and *Smirnov* [9.36, 37] developed the "method of the transient processes" for the investigation of the stationary state. This method is based on the following. In the stationary state the system of parametric waves is at equilibrium with the pumping field. The change in the pumping parameters (phase, frequency, amplitude), which is fast in comparison with the lifetime of waves, leads to the violation of the equilibrium and to the change in the absorbed power. Then a certain transient process is observed and over the time $\tau = 1/2\gamma$ the system reaches the stationary state again. The reaction of the parametric waves system to the parameter change reveals to us the information about the properties of the stationary state including the phase of parametric waves.

Experiments were performed on the antiferromagnetic easy-plane $MnCO_3$ at the pumping frequency $\omega_p/2\pi = 35.5$ GHz and at the temperature of the liquid helium [9.36]. The pumping phase was rapidly changed in the following way a short pulse ($\tau_p \simeq 0.1$ ms) was sent to the klystron repeller plate. During the pulse time the klystron generated with a frequency differing from ω_p by $\Delta\omega_p$. Thus, following this pulse, the phase of the microwave signal was shifted with respect to its initial phase by the amount $\beta \simeq \Delta\omega_p\tau_p$. It appeared that parametric magnons respond to the pumping change phase depending on β. Immediately after the phase-rotating pulse the absorbed power can either be more or less than in the stationary state. Moreover, at definite values β the spin system radiates, delivering the energy to the resonator. Then, during a time of approximately 1 ms, the system returns to the stationary state. By the reaction to the pumping phase change, the stationary phase of the parametric spin waves Ψ was found. Fig. 9.10 shows the results of the performed experiment: the change in the absorbed power in the sample versus the pumping phase change β. It follows from the analysis of these results that Ψ differs from the optimum one (corresponding to the maximum power selection) the larger the ratio h_{th}/h. This weakens the connection with the pumping and, consequently limits the amplitude of parametric waves. The obtained parametric dependence $\Psi(p)$ is shown in Fig. 9.11. Similar experiments on YIG were carried out by *Melkov* and *Krutsenko* [9.24] and also by *Prozorova* and *Smirnov* [9.36]. Their results are shown in the same figure.

It is clear that within the experimental error the points are located at the bisector of the coordinate angle as follows from (5.5.7) for antiferromagnets and (5.5.12) for ferromagnets in the state with a single group of pairs.

It confirms the validity of the S-theory for the correct description of the significant aspects of the above-threshold behavior of parametric waves. The deviation of the results for YIG at the supercriticality over 10 dB ($h > 3h_{th}$)

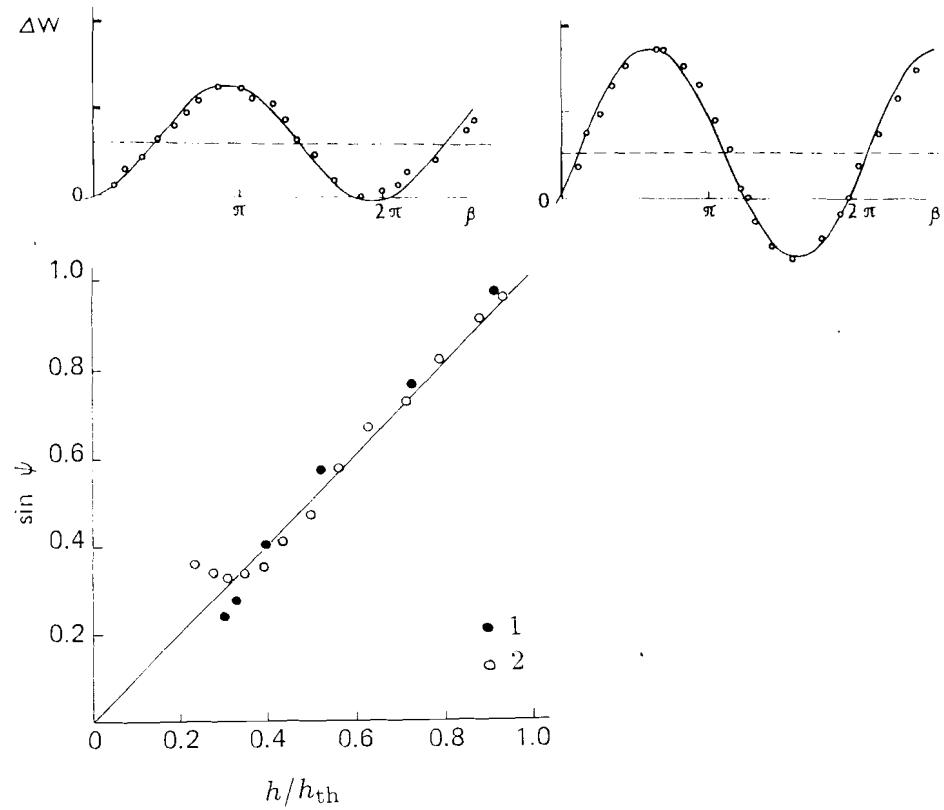

Fig. 9.10. (above) Variation in the power ΔW absorbed by $CsMnF_3$ versus variation of the pump phase. (A) $h/h_{th} = 1.08$; (B) $h/h_{th} = 2.25$, $T = 1.62$ K, $H = 2.25$ kOe (*Prozorova, Smirnov* [9.36])

Fig. 9.11. (below) Stationary phase Φ of a pair versus supercriticality. (1) results of an experiment conducted on $CsMnF_3$ monocrystals at $T = 1.62$ K and $H = 2.55$ kOe (*Prozorova* and *Smirnov* [9.36]). (2) Results for YIG sphere, 2 mm in diameter, $\boldsymbol{H} \parallel [100]$, $H = H_c - 500$ Oe (*Melkov* and *Krutsenko* [9.24])

from the simple formula (5.5.12) is associated with the excitation of the second group of pairs with $\Theta = \pi/2$. This phenomenon was described in Sec. 5.5.3 of the basic S-theory. Its experimental confirmation will be given in Sec. 9.6.

9.4 Electromagnetic Radiation of Parametric Magnons

The investigation of the radiation of parametric magnons is of interest, first of all, because it enables us to determine their spectrum, i.e. the value

$$N(\omega) = \int n_{\mathrm{p}}(\boldsymbol{k}, \omega)\, d\boldsymbol{k} \ . \tag{9.4.1}$$

It must be noted that the direct electromagnetic radiation of the parametric magnons with $k \simeq 10^4$–10^6 cm^{-1} is extremely weak because of the momentum conservation $k_{\mathrm{p}} \ll k$. Nevertheless, recently manufactured modern microwave equipment has made possible such investigations.

9.4.1 Frequency of Parametric Magnons

From the conservation laws

$$\omega(\boldsymbol{k}) + \omega(-\boldsymbol{k}) = \omega_{\mathrm{p}} \tag{9.4.2}$$

it follows that magnons are parametrically excited at a frequency equal to half the pumping frequency. However, an important question remains about the accuracy with which the conditions (9.4.2) are satisfied in experiment. Are only magnons with the frequency $\omega(\boldsymbol{k})$ excited exactly equal to $\omega_{\mathrm{p}}/2$? Does the spectral distribution $n(\omega(\boldsymbol{k}))$ really have the form of the δ-function? Or does excitation occur in some frequency band $\delta\omega(\boldsymbol{k})$? The fact that the excited magnons have the frequency $\omega(k) = \omega_{\mathrm{p}}/2$ can be confirmed with a certain accuracy by the region of existence of additional absorption (if it exists) or from the experimentally observed peculiarity of parametric magnon relaxation at the intersection point of the magnon and (known from other experiments) phonon spectra [9.7–9]. The frequency of parametric magnons with $k \simeq 10^4$–10^6 cm^{-1} can be obtained with more accuracy in the experiments on Mandelstam-Brillouin scattering of light on these magnons [9.38, 39]. However, the error in determining the frequency of magnons in these experiments (1 GHz) is still too large for measuring $\delta\omega(k)$.

The most direct and accurate method of obtaining the spectral distribution of parametric magnons is to study the spectrum of the resulting radiation $I(\omega)$. We readily have:

$$I(\omega) = 8\omega^4(k) M |\Delta M| N(\omega) / 3c^3 k^2 V^{2/3} \ , \tag{9.4.3}$$

where ΔM is the magnetization change when one magnon is excited. Interestingly, in antiferromagnets with weak ferromagnetism ($H_{\mathrm{D}} \neq 0$) this value can significantly exceed the Bohr's magneton μ_{B}. Indeed,

$$\Delta M = -\hbar \frac{\partial \omega(k)}{\partial H} = -\frac{g(H + H_{\mathrm{D}})}{2\omega(k)} \mu_{\mathrm{B}} \ . \tag{9.4.4}$$

Therefore, in order to observe radiation, it is convenient to increase the pumping frequency and use substances with a large value of H_{D}.

The study of parametric magnon radiation was carried out by *Kotuzhansky* et al. [9.41, 42]. The monocrystals of $FeBO_3$ were used (cylindrical samples with a diameter 2 mm and a height of 3 mm). The axis of the cylinder coincided with the principal axis of the crystal. The microwave pumping was produced by the continuous-action magnetron oscillator with the frequency $\omega_{\mathrm{p}}/2\pi = 35.6$ GHz and 10 W power. The cylindrical resonator of the transmission-type microwave spectrometer was tuned so that the frequency of its mode TE_{012} coincided with ω_{p}. The samples are placed in the exit coupling window of the resonator symmetrically about its wall with the thickness of 0.5 mm. Therefore, one part of the sample protruded into the standard waveguide at 1.5 cm of the microwave range. The fields $\boldsymbol{h}$ and $\boldsymbol{H}$ were in the basal plane of the crystal and were parallel to each other. The signals with the frequencies ω_{p} and $\omega_{\mathrm{p}}/2$ were separated by the microwave filters. The decoupling between the channels was 40 dB. The signal at the frequency $\omega_{\mathrm{p}}/2$ was received by a superheterodyne receiver with the sensitivity 10^{-14} W and was analyzed by the spectrum analyzer.

It was experimentally found that above the threshold of the parametric excitation as the microwave pumping power is absorbed at the frequency ω_{p} simultaneously appears the radiation from the sample at the frequency $\omega_{\mathrm{p}}/2$. The radiation intensity $I(\omega)$ depended on time in a random manner. The oscillogram of the output signal from the receiver had the form of splashes with duration $\tau \simeq 10^{-5}$–10^{-6} s. The principally important result of the experiment was the fact that the center of the radiation band coincided with $\omega_{\mathrm{p}}/2$ with the accuracy $\pm 2\pi \cdot 20$ kHz, i.e. with the relative accuracy of the order of 10^{-6}. This was proved as follows: The radiation signal and the signal from the additional microwave klystron oscillator, which was tuned such that its second harmonics coincided with the pumping frequency, were simultaneously applied to the output of the receiver. The klystron was tuned to the zero beats of voltage from the microwave detector where the signals from the klystron and magnetron became detuned. Within the error of the frequency measurement due to the parasitic deviation of the klystron and magnetron frequencies, the klystron frequency coincided with the radiation frequency.

9.4.2 Frequency Width of Parametrically Excited Magnons

1 Limitation of the number of magnons by nonlinear damping in the easy-plane antiferromagnet $FeBO_3$ The previously cited paper (*Kotyuzhansky* et al. [9.41]) also discusses the shape of the wave packet $N(\omega)$. It was found that the width of the wave packet $\Delta\omega$ increases linearly with h/h_{th} (see Fig. 9.12). The broadening of the radiation line, $N(\omega)$, in $FeBO_3$ was investigated theoretically by *Mikhailov* and *Chubukov* [9.42]. The theoretical estimate of the linewidth $\Delta\omega$ obtained in this paper is by a factor of 25

less than the experimentally observed value. The form of the h-dependence of $\Delta\omega$ obtained by *Mikhailov* and *Chubukov* [9.42] coincides with the experimental data only for $p > 16$. This disagreement is evidently due to certain simplifications in the theory [9.42]. In particular, the assumption of the equilibrium of the photons. As shown by *L'vov* [9.43], the shape of the wave packet $N(\omega)$ is not determined by any specific mechanism of nonlinear damping and is obtained in accordance with (6.4.16) by the general structure of the Green's function (6.4.15). *Mikhailov* and *Chubukov* [9.42] showed (see Fig. 9.13) that the experimentally observed line shape $N(\omega)$ coincides with the theoretical data (See (6.5.26), *L'vov* [9.43]).

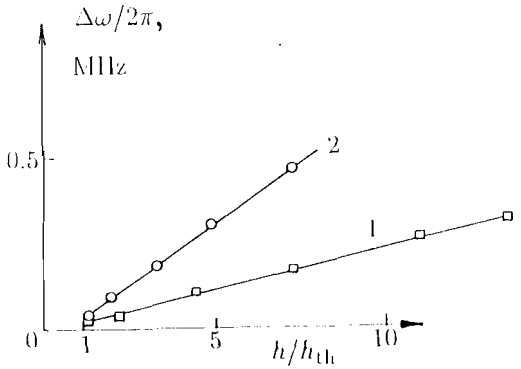

Fig. 9.12. Magnon radiation linewidth in $FeBO_3$ versus pumping amplitudes for $H = 380$ Oe. (Width was measured at the level 0.1 I_{max}). (1) T=1.2 K; (2) T=4.2 K (*Kotyuzhancky* et al. [9.41])

2 Limitation of the number of magnons by phase mechanism in the ferromagnet YIG. *Krutsenko, L'vov* and *Melkov* [9.44] applied another procedure in order to investigate the shape of the wave packet $N(\omega)$ in YIG. To this end, electromagnetic radiation from the ferrite was recorded at the frequencies close to half pumping frequency. This phenomenon is due to the two-magnon scattering of parametric magnons by static inhomogeneities. In this case for the complex envelope of the electromagnetic wave $U(t)$ which is radiated by the crystal one has

$$U(t) = \sum_{\mathrm{n}} \int g(\boldsymbol{k}) \exp(i\boldsymbol{k}\boldsymbol{r}_{\mathrm{n}}) a(\boldsymbol{k}, t) d\boldsymbol{k} \ , \tag{9.4.5}$$

where $g(\boldsymbol{k})$ is the transformation amplitude of the magnon with $\boldsymbol{k} = 0$ into a homogeneous oscillations mode (magnons with $\boldsymbol{k} = 0$) on a single scattering center, $\boldsymbol{r}_{\mathrm{n}}$ denote the coordinates of these centers. By employing (9.4.5) we obtain the expression for the correlation function of the radiation $K(\tau)$

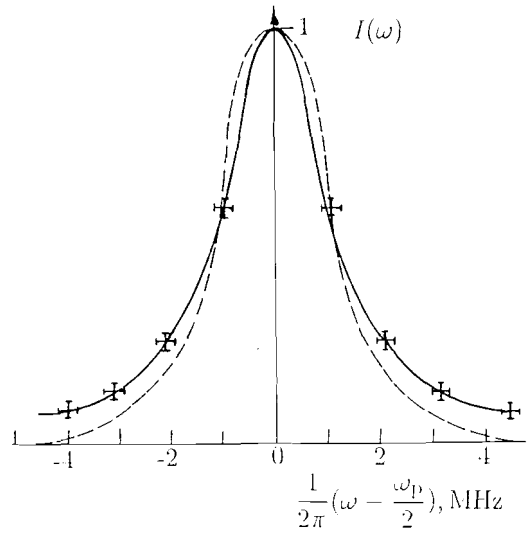

Fig. 9.13. Magnon radiation lineshape in $FeBO_3$. The solid line is the theoretical relation (calculated from equations given by the author [9.43] and later by *Mikhailov* and *Chubukov* [9.42]), in which the half-width is taken equal to the experimentally observed value (*Kotyuzhansky* et al. [9.41]); the dashed line is a Lorentzian of the same width

$$K(\tau) = \langle U(t)U^*(t+\tau)\rangle = N_{\mathrm{def}} \int |g(\boldsymbol{k})|^2 n(k,\tau)\, d\boldsymbol{k} \ . \tag{9.4.6}$$

Here N_{def} is the number of scattering centers, $n(\boldsymbol{k}, \tau)$ designate the different-time correlation function of magnons; $n(\boldsymbol{k}) = n(\boldsymbol{k}, \tau)$ at $\tau = 0$. From (9.4.6) it can be seen that with the accuracy of the time-independent scale factor, the function $K(\tau)$ is equal to the correlation function of magnons integrated over k: $N(\tau) = \int n(\boldsymbol{k}, \tau)\, d\boldsymbol{k}$, and therefore the spectral density $K(\omega)$ differs from the spectral density of the magnons $N(\omega)$ specified by relation (9.4.1) only in the constant factor. This conclusion is essentially due to the fact that the two-magnon scattering by the static inhomogeneities is not accompanied by the change in oscillation frequency. Thus, the static properties of parametric magnons can be investigated by treating the electromagnetic radiation from the ferrite.

The samples used in experiments [9.44] were ferrite spheres made of YIG monocrystals, 2.5 to 2.9 mm in diameter. They were studied at room temperature. The pumping frequency $\omega_{\mathrm{p}}/2\pi = 9.37$ GHz. The spheres were oriented along the hard direction of magnetization [100] $\parallel \boldsymbol{H}$ to exclude the effect of the low-frequency self-oscillations of the magnetization. The electromagnetic radiation from the ferrite is maximum when the frequency of this radiation is equal to the frequency of one of the magnetostatic modes. The registering circuit consisted of a 6 cm-range amplifier, protected against the pumping frequency by a low frequency filter, a square-law detector and

a spectrum analyzer of single-frequency range. Fig. 9.14 shows the typical dependence $I(\epsilon)$, $\epsilon = (\omega - \omega_p/2)$, obtained experimentally on one of the studied YIG spheres. The solid curve in Fig. 9.14 is the result of averaging over 10 realization of stochastic process.

In order to determine the type of the experimental curve $I(\epsilon)$, it was plotted on the various rectified coordinates. If $I(\epsilon)$ is a Gaussian curve it will be a straight line on the coordinates $\sqrt{\ln(1/I)}, \epsilon$; if $I(\epsilon)$ is a Lorentzian curve this yields the straight line on the coordinates $\sqrt{1/I - 1}, \epsilon$; if $I \sim \sqrt{\epsilon/\mathrm{sh}\epsilon}$ the straight line will be a result of the dependence $I(\epsilon)$ plotted on the coordinates $\ln[1/I + \sqrt{1/I^2 - 1}]$. As can be seen from Fig. 9.14, the first standard functions are completely unsuitable for the description of the experiment, at the same time the function $\sqrt{\epsilon/\mathrm{sh}\epsilon}$ is in satisfactory agreement with the experiment. Such a coincidence of the shape of the curve $I(\epsilon)$ was observed for all the studied samples at different supercriticalities and values of the constant magnetic field. The slope tangent of the straight line 3 in Fig. 9.14 determines the width of the curve $\Delta\epsilon$ which because of the peculiarities of the quadratic detector is $\sqrt{6}$ times as large as the real width of the electromagnetic radiation curve $\Delta\omega$ coinciding with the width of the spectral density of parametric magnons. Fig. 9.15 shows the distribution width of parametric magnons $\Delta\omega$ versus the supercriticality $p = (h/h_{\mathrm{th}})^2$. The results obtained are in good agreement with the S, T^2-theory which will be considered in Sec. 10.2.

9.5 Collective Resonance of Parametic Magnons

This section deals with homogeneous collective oscillations, i.e. the simplest type of the oscillations corresponding to the gap in their spectrum. The resonance in the system of parametric magnons resulting from the excitation of homogeneous collective oscillations is very intense and can therefore be observed more readily. *Zautkin* and *Starobinets* [9.46] observed experimentally the reaction of the sample to the additional alternating field with the frequency $\omega_p \pm \Omega$ under parallel pumping of magnons in YIG monocrystals. The mixing of this field with the pumping field at the frequency ω_p in the nonlinear system brings about a signal of low combinatorial frequency Ω which results in the collective resonance of parametric magnons. The resonance was detected by the peaks which appeared in the absorption spectrum of the weak signal and from oscillation excitation of the longitudinal magnetization of the sample at a low frequency.

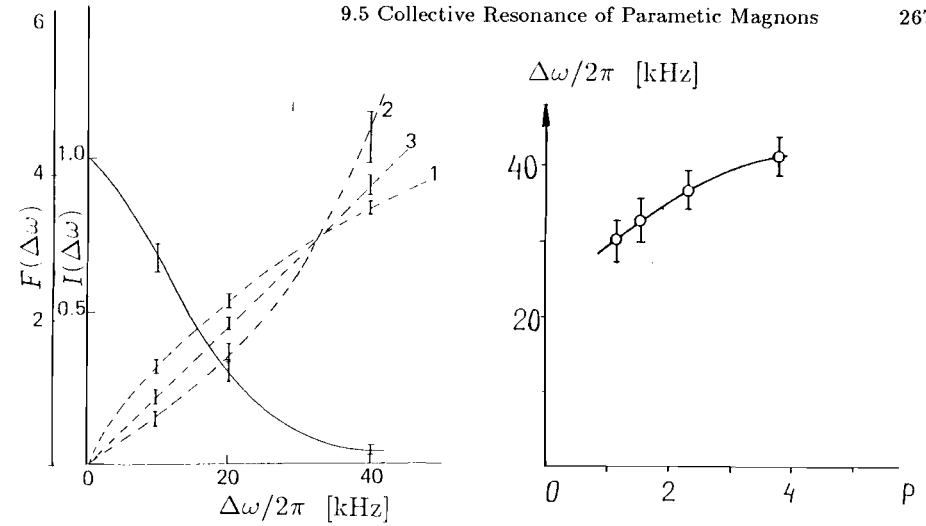

Fig. 9.14. (left) Solid line: spectral power $I(\epsilon)$ of the parametric magnon radiation (YIG sphere, $\Delta H(k) = 0.15$ Oe, $p = 6$ dB). Dashed curve: build-up of $I(\epsilon)$ in the coordinates: (1) $F(\epsilon) = 2\sqrt{-\ln I(\epsilon)}$; (2) $F(\epsilon) = \sqrt{I^{-1}(\epsilon) - 1}$; (3) $F(\epsilon) = \ln[I^{-1}(\epsilon) + \sqrt{I^{-2}(\epsilon) - 1}$ (After *Krutsenko* et al. [9.44])

Fig. 9.15. (right) Width of the parametric magnon radiation $\Delta\omega/2\pi$ versus pumping power p for YIG sphere (After *Krutsenko* et al. [9.44])

9.5.1 Experimental Technique

Figure 9.16 shows the experimental setup for observing the resonance of collective oscillations of parametric magnons. The rectangular resonator was connected by two holes with two waveguide channels over which two microwave signals were transferred to the sample. One of them, namely the powerful magnetron pulse at the frequency $\omega_p = 2\pi \cdot 9.37 \cdot 10^9$ s^{-1}, was employed as usual for parallel pumping of magnons and the second one was an additional weak signal whose magnetic field was polarized to the constant field and the pumping field. As a source of the weak signal a klystron with 3 cm range of wave length was used. The pulses of the sawtooth voltage of the oscillograph sweeping (which is turned on simultaneously with the pulse of the intense pumping sent to the sample) were sent to the klystron repeller plate. As a result, over the time of the pumping influence the frequency of the weak signal changed within a small range from $\omega_p - \Omega$ to $\omega_p + \Omega$, whose limits were regulated by the sweep generator from zero to several MHz. The central frequency at the same time corresponded to the peak of the klystron generation zone and was selected equal to the frequency of pumping and the eigenfrequency of the resonator in its operation mode. The sweeping duration of the weak signal with respect to frequency corresponded to the duration of the pumping pulse (10^2–10^4ms at the repetition frequency 25 Hz). After passing through the resonator with the sample the weak signal came to the directional coupler, connected with the waveguide channel of

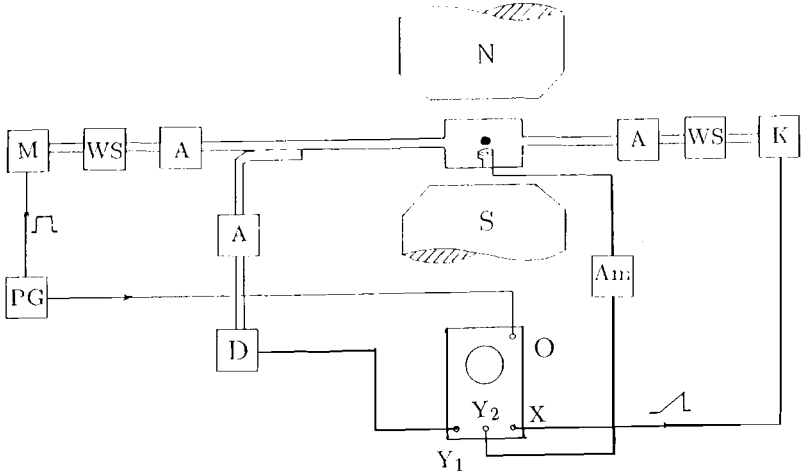

Fig. 9.16. Block diagram of experimental setup for investigations of collective resonance of parametric magnons (*Zautkin* et al. [9.46]). M, magnetron; K, klystron; PG, pulse generator; WS, waveguide switch; A, attenuator; R, cavity resonator; D, cristal detector; Am, amplifier; O, oscillograph.

the magnetron; then it was registered and observed on the screen of the oscillograph as a curve proportional to the plot of the amplitude of passage through the resonator versus frequency $D^2(\omega + \Omega)$. Below the threshold of the parametric excitation of the spin wave the oscillogram have a shape of an ordinary resonance curve of the resonator on the peak of wich there are zero beats indicating that at the moment (at the given point of the oscillogram) the frequencies of the magnetron and klystron are equal ($\Omega = 0$). Above the threshold the resonance curve is overlapped by the absorption spectrum of the weak signal due to its interaction with the system of parametric magnons. In order to facilitate the observation of the passing signal the repelled signal was successfully decreased to a level not exceeding 10% of the useful signal reaching the detector by means of matching the resonator with the waveguide.

For the registration of the oscillation variation at low frequency a detector coil was placed into the resonator near the sample, the axis of the pumping was parallel to the constant magnetic field. At the oscillating longitudinal magnetization in the signal is induced in the coil. After the amplification by the low-noise amplifier this signal was transmitted to the second channel of the oscillograph and simultaneously registered with the absorption spectrum of the weak channel. The observation and measurements were performed on several YIG samples shaped as discs and spheres at different orientations of the external magnetic field with respect to its crystallographic axes. Most interesting are the measurements at the orientation along the axis [100] when above the threshold up to the supercriticalities

9 dB in the system of parametric magnons there are no auto-oscillations of the magnetization.

Figure 9.17 shows the oscillograms of the frequency dependences of the coefficient of the weak signal passage through the resonator $D^2(\omega + \Omega)$ and of the oscillations of the longitudinal magnetization $m_z(\Omega)$. The oscillograms were obtained at different fixed supercriticalities of pumping. It can be seen that immediately above the threshold a comparatively narrow absorption peak appears on the curve $D^2(\omega + \Omega)$. This peak increases as the pumping power increases and is shifted towards higher frequencies. Simultaneously with the absorption peak the resonance increase of the low-frequency oscillations amplitude is observed on the oscillograms $m_z(\Omega)$, the maximum of the amplitude showing the behavior similar to the absorption spectrum. Such a simple picture is observed up to the supercriticalities of the order of 9 dB. At large pumping power the spectrum is significantly distorted: the intense peak is broadened, new peaks appear in the vicinity of the center frequency, on the oscillogram $m_z(\omega)$ there appear respective additional symmetrical maxima. This mode is accompanied by the emergence of chaotic auto-oscillations modulating the reflected pulse of the magnetron and hindering the isolation of peaks in the spectrum $D^2(\omega + \Omega)$. It must be noted that the complex absorption spectrum is observed also in the case $\boldsymbol{M} \parallel [111]$, when immediately above the threshold intense auto-oscillations are excited.

9.5.2 Frequency of Collective Resonance

Let us obtain the resonance frequency of the collective oscillations Ω_{res}. It can be found through direct measurement of the absorption peak shift from the center frequency on the oscillogram $D^2(\omega + \Omega)$. Fig. 9.18A plots the measured resonance frequency versus the pumping intensity for two values of the constant field. The dependences prove to be linear within a wide range of supercriticalities corresponding to one peak in the absorption spectrum of the weak signal. The slope of the plots in Fig. 9.18A increases as the constant field decreases.

The experimental dependence of the resonance frequency on the constant field is shown in Fig. 9.18B for the supercriticality $p = 4$ dB. In order to verify the assumption of the space homogeneity of the excited oscillations based on the high intensity of the observed resonance, the dependences of the resonance frequency on the constant field were measured on the samples shaped as spheres of different diameter. Fig. 9.18B confirms this assumption because the collective oscillations are practically not influenced by the size of the crystal, they do not "feel" the boundaries of the sample.

Figure 9.18C shows the experimental data which enable one to form an opinion about the influence of the sample shape on the resonance frequency of collective oscillations. The curves were obtained on the YIG samples shaped as a sphere and disc, the direction of the sample magnetization was

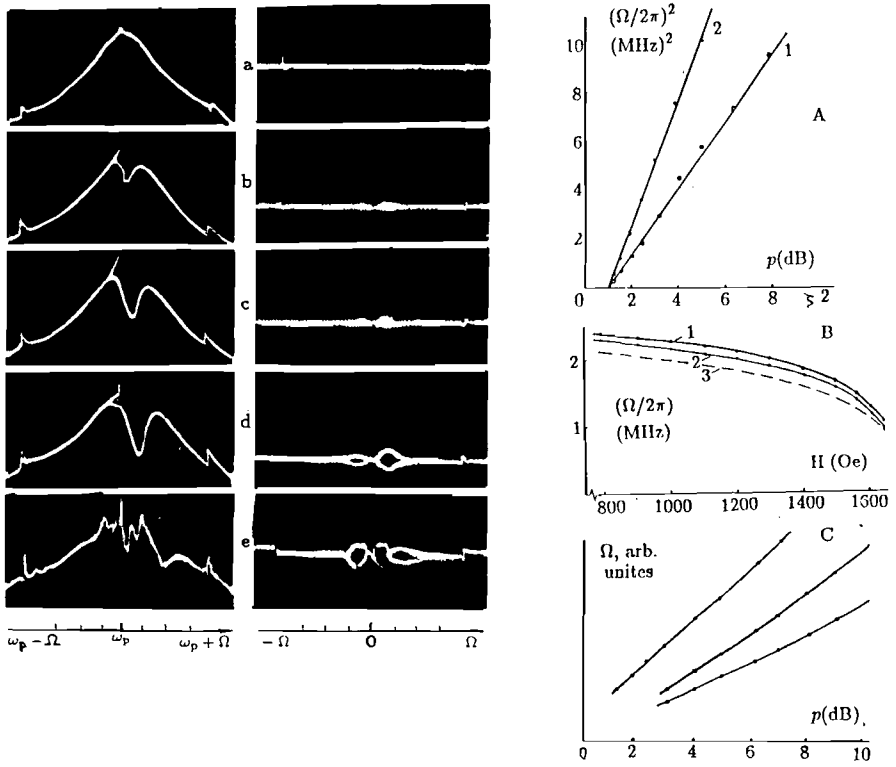

Fig. 9.17. (left) Oscillograms of the frequency dependences: of the coefficient of weak signal passage through the resonator (on the left), of the amplitude of longitudinal magnetization (on the right) under different pumping power; (a) 0 dB, (b) 2 dB, (c) 4 dB, (d) 6 dB, (e) 13 dB. The speed of the oscilloscope unfold was 1.5 MHz /point (*Zautkin* et al. [9.46])

Fig. 9.18. (right) [A] Resonant frequency of collective oscillation versus supercriticality for YIG sphere at $\boldsymbol{M} \parallel [100]$ and different value of magnetic field: (1) $H_c - H = 100$ Oe, (2) $H_c - H = 300$ Oe.
[B] Resonant frequency of collective oscillation versus magnetic field for YIG spheres at $p = 4$ dB, $\boldsymbol{M} \parallel [100]$ and diameters $d = 1.002$ mm (plot 1), $d = 1.56$ mm (plot 2); plot 3 is the result of calculation according to (7.4.1b) and (7.1.5) at $m = 0$.
[C] Theory (lines) and experiment (dots) for resonant frequency of collective oscillation versus supercriticality for YIG at $\boldsymbol{M} \parallel [100]$: plot 1 at $N_z = 0$ (disc), plot 2 at $N_z = 1/3$ (sphere), plot 3 at $N_z = 1$ (disc). After *Zautkin* et al. [9.46]

selected everywhere along the axis [100] in order to avoid the influence of its crystal anisotropy on the comparison of results. All three curves were measured at the same values $(H_c - H)$, which ensured the equality of the wave numbers of spin waves. The very fact of the sample shape influence on Ω_{res} is not surprising because this influence is experienced, as we have already seen, also by the amplitudes of the interaction Hamiltonian of parametric magnons S_0 and T_0 which determine the eigenfrequency of collective oscillations Ω_0 in the system.

To explain these experiments let us employ the theory of collective oscillations developed in Sect. 7.1.2. As can be seen from (7.2.10) for the nonlinear susceptibility to the weak signal $\chi''(\omega_p + \Omega)$ the resonance frequency Ω_{res} differs from the eigenfrequency Ω_0 of the collective oscillations by the value of the order γ^2/Ω_0 which under the considered experimental conditions is 0.1 MHz at $p = 1.5$ and rapidly decreases as the supercriticality increases $(\gamma^2/\Omega_0^2 \simeq 1/4p)$. Therefore we can compare the measurement results with the simple formula (7.1.4), which, if we allow for the well-known dependence $N(p)$ (5.5.7) assumes a convenient form

$$\Omega_0^2 = 4\gamma^2[1 + 2T_0/S_0](p - 1) \,. \tag{9.5.1}$$

The linear dependence of the squared eigenfrequency of the collective oscillations on the supercriticality is confirmed by the straight-line experimental plots in Fig. 9.18A. The slope of the plot, say, for $H_c - H = 100$ Oe, equal to $(1.5 + 0.2)$ MHz is in good agreement with the theoretical value

$$\partial(\Omega_0)^2/\partial p = 4\gamma^2[1 + 2T_0/S_0] = 1.33 \text{ MHz} \,.$$

In the last estimation the value $T_0/S_0 = 0.54$ was employed founded from (7.1.5) and the value $\gamma = 0.4$ MHz calculated from the absolute measurements of the threshold of parametric magnons.

Formula 9.5.1 naturally explains the field dependence of the resonance frequency of collective oscillations of parametric magnons by the dependence of the damping parameter of spin waves $\gamma(k)$ on their wave number k determined by the value of the constant field. In order to compare the experimental and theoretical data, the dependence $\Omega_0(H)$ is plotted in Fig. 9.18B, calculated from (9.5.1) allowing for the real values of $\gamma(k)$ obtained from the threshold measurements $h(H)$. With an accuracy of 10% the calculation gives correct values of the resonance frequency over the entire studied field range.

By calculating T_0/S_0 from (7.1.5) one can obtain from (9.5.1) the resonance frequencies of collective oscillations of parametric waves for the disc magnetized parallel to the plane of the sphere and the disc magnetized perpendicular to the plane. Calculation shows that these frequencies relate as $3.4 : 2.3 : 1$ respectively. The same type of influence of the sample shape on was also observed experimentally (see Fig. 9.18C).

Formula (9.5.1) thoroughly verified and experimentally validated enables us to suggest the resonance method of obtaining the relaxation parameter of spin waves $\gamma(k)$ at known value of T_0/S_0. And on the contrary, if $\gamma(k)$ is known, relation (9.5.1) allows to obtain experimentally the important parameter T_0/S_0 characterizing the interaction of pairs of spin waves above the threshold of the parametric excitation.

9.5.3 Susceptibility to Field of Weak Microwave Signal

Measurements show that the intensity of the absorption on the curve $D^2(\omega_p + \Omega)$ is strictly proportional to the intensity of the weak signal. This circumstance enables us to introduce the susceptibility of the parametric magnon system at the frequency of the weak signal $\chi''(\omega_p + \Omega)$ as the ratio of the absorbed intensity of this signal to the intensity incident on the sample from the klystron. This susceptibility can be experimentally obtained from the form of the frequency dependence of the coefficient of passage through the resonator [9.23]. Fig. 9.19 shows measurement results for the susceptibility to the weak signal field as a function of the pumping supercriticality. The susceptibility $\chi''(\omega_p + \Omega)$ is represented in terms of the susceptibility to the main pumping χ'' because this susceptibility provides a natural scale for their comparison. The dependence proves to be linear, and the numeric values are rather large (at $p = 8$ exceeding the value of χ'' more than by an order of magnitude, which is in agreement with the assumption of intense homogeneous collective oscillations).

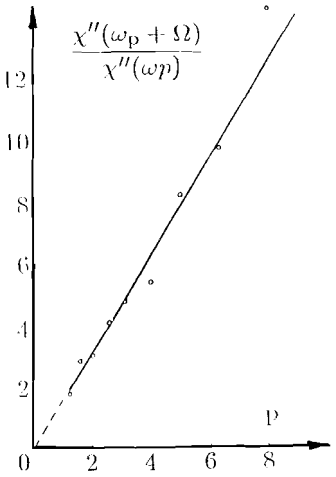

Fig. 9.19. Susceptibility to weak RF signal $\chi(\omega_p + \Omega)$ over susceptibility to pumping $\chi(\omega_p)$ versus supercriticality p for YIG sphere at $M \parallel [100]$, $H_c - H = 100$ Oe. After *Zautkin* et al. [9.46]

According to the theory developed in Sec. 7.2, the susceptibility to the weak signal must have a resonance character (7.2.10) with the maxima near $\omega_p \pm \Omega$ and the halfwidth γ. At the resonance points $\chi''(\omega_p \pm \Omega)$ is given by (7.2.11). Thus, the resonance susceptibility $\chi''(\omega_p + \Omega)$ is p times as large as the susceptibility to the pumping with respect p to the order of magnitude. This fact is also manifested experimentally. From Fig. 9.19 it can be seen that the ratio $\chi''(\omega_p + \Omega)/\chi''$ near the threshold is equal to 2 and at p=8 is 14.

According to the theory (7.2.11) the experimental dependence $\chi''(\omega + \Omega)/\chi''$ on the supercriticality of the magnon system p is linear. The theoretical value of the slope equals to 2 at $T_0/S_0 = 0.54$ (7.1.5) is in agreement with the experimental value 1.65 for the plot in Fig. 9.19.

Asymmetry of absorption spectrum of weak signal (see Fig. 9.17) is the peculiarity of the collective resonance of spin waves. This fact can be easily accounted for theoretically. As follows from (7.2.11), the signs of susceptibilities of $\chi''(\omega_p + \Omega)$ and $\chi''(\omega_p - \Omega)$ are different. This means that at the frequency $(\omega_p + \Omega)$ the absorption takes place, and at the frequency $(\omega_p - \Omega)$ the weak signal is amplified (at positive T and S). The magnitudes of these susceptibilities in accordance with (7.2.11) also differ greatly. At $T_0/S_0 = 0.54$ (YIG sphere) the amplification turns out to be much less than the absorption $\chi''(\omega_p - \Omega)/\chi''(\omega_p + \Omega) = -0.03$ and therefore cannot be registered on the background of the resonance curve of the coefficient of the passage through the resonator.

9.5.4 Linewidth of Collective Resonance

Measurements by *Zautkin* et al. [9.46] show that within the experimental accuracy the resonance width of collective oscillations is independent of the pumping intensity up to the supercriticality $p \simeq 9$ dB. Fig. 9.20 shows the dependence of the frequency width of resonance (measured on the oscillograms $D^2(\omega + \Omega)$) on the constant field. According to theory (see (7.2.10) the resonance halfwidth which determines the damping of collective oscillations proved to be equal to the parametric spin damping of waves making up the collective modes of oscillations. This fact was experimentally confirmed in Fig. 9.21 where the dependences of the magnon relaxation frequencies on the external magnetic field are plotted based on the experimental measurements of their threshold (curve 1) and of the collective resonance width (curve 2). These curves coincide within the limits of experimental error. Therefore the measurement of the width of the absorption peak $D^2(\omega + \Omega)$ under the immediate observation of its shape on the screen of an oscillograph provides an illustrative method for obtaining the relaxation time of spin waves. It is important that this method involves no absolute measurements of the microwave field inside the sample, which is a difficult task in the general case.

Since the damping γ, as is known [9.13, 15, 47], increases linearly as the number of magnons increases, according to the above stated correspondence a similar linearity with respect to k should be expected for the linewidth of the collective resonance. The experimental plot of the field dependence of the linewidth (Fig. 9.20) also points to its dependence on k, at the same time the value γ plotted in Fig. 9.21 as a function of $\sqrt{H_c - H} \sim k$ really proves to be linear.

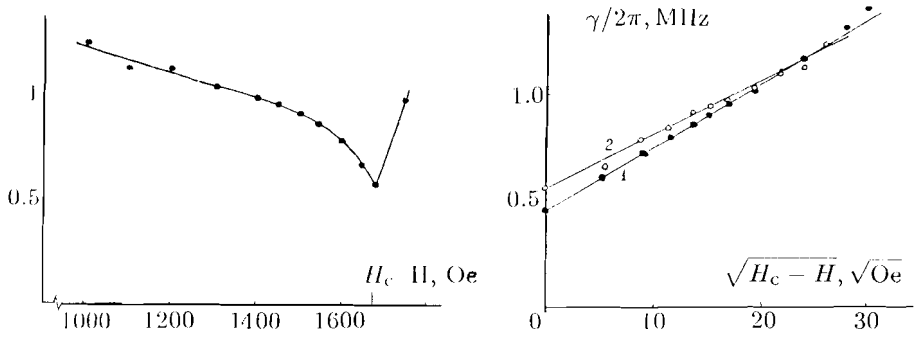

Fig. 9.20. (left) Frequency width of collective resonance of parametric magnons in YIG sphere versus magnetic field at $M \parallel [100]$. After *Zautkin* et al. [9.46]

Fig. 9.21. (right) Frequency of magnon damping in YIG sphere versus magnetic field at $M \parallel [100]$, obtained from parametric threshold data (curve 1) and from data for width of collective resonance (curve 2). After *Zautkin* et al. [9.46]

9.5.5 Oscillations of Longitudinal Magnetization

The dependence of the oscillation amplitude of the longitudinal magnetization registered by e.m.f. in the induction coil on the frequency of the weak signal and supercriticality is qualitatively characterized by a set of oscillograms in Fig. 9.17. Quite surprising is the drastic difference in the behavior of $m_z(\pm\Omega)$ and $D^2(\omega_p \pm \Omega)$ which consists, as becomes clear from Fig. 9.17, in the fact that once more a lower maximum of $m_z(-\Omega_{res})$ corresponds to the resonance $m_z(+\Omega_{res})$, at the same time the absorption peak $D^2(\omega_p + \Omega_{res})$ has no symmetrical satellite at the frequency $\omega_p - \Omega_{res}$.

Fig. 9.22 plots the intensity of low-frequency oscillations versus the intensity of the weak signal. The plot shows that within the measurement range the oscillations are linear with respect to the field of the signal exciting these oscillations. This fact enables us to simplify the task of the development of collective resonance theory and to confine ourselves to the linear approximation for the oscillation amplitude of the wave amplitude with respect to the stationary state.

In order to find $m_z(\Omega)$, in (3.4.8) for the longitudinal magnetization, value $a(\boldsymbol{r}, t)$ must be expressed in terms of $a(\boldsymbol{k}, t)$. Then the circular canonical variables $a(\boldsymbol{r}, t)$ must be expressed in terms of to the normal canonical variables of the quadratic Hamiltonian. Subsequently we must substitute into the obtained expression the expansion (7.2.7) and retain only the relevant for us resonant terms proportional to $\exp[-i\Omega t]$ to oscillate with the low frequency Ω. As a result, we obtain in linear approximation with respect to the amplitude of the weak signal:

$$m_z(\Omega) = U_0[c_0^* d(\Omega) + c_0 d^*(-\Omega)] \,. \tag{9.5.2}$$

Here $U_0 \simeq g$ is given by (7.2.4), $|c_0|^2 = N$ denotes the total number of parametric magnons, $d(\Omega)$ is specified by (7.2.3, 7). By employing all these formulae we readily obtain from (7.2.8)

$$m_z(\Omega) = U_0 N \frac{h_s}{h_{th}} \frac{\gamma[\Omega + 2S_0 N - 2i\gamma]}{\Delta_0^2 - \Omega^2 - 2i\gamma\Omega} \,, \tag{9.5.3}$$

Here h_s is the amplitude of the weak signal with the frequency $(\omega_p + \Omega)$, $\Delta_0 = 2N\sqrt{S_0(2T_0 + S_0)}$ designates the frequency of the collective resonance. As it should be expected the amplitude $m_z(\Omega)$ is at maximum if $\Omega = \pm\Delta_0$. From (9.5.3) an expression for the ratio of the resonance maxima at the image frequencies $\omega_p \pm \Omega$ can be obtained:

$$\frac{m_z(\Delta_0)}{m_z(-\Delta_0)} = \sqrt{\frac{1 + 2(p-1)[1 + t + \sqrt{1+2t}]}{1 + 2(p-1)[1 + t - \sqrt{1+2t}]}} \,. \tag{9.5.4}$$

Here $t = T_0/S_0 \simeq 0.54$ under experimental conditions (YIG sphere, $M \parallel [100]$). At $p = 2$, for example, ratio (9.5.4) equals 2.4 which is in agreement with the experimental value of the ratio of the maxima, equal to 2.

The consistent explanation (from the same position) of the weak asymmetry $m(\pm|\Omega|)$ and the strong asymmetry $\chi''(\omega_p \pm |\Omega|)$ is a significant merit of the statement about collective resonance of parametric magnons developed in Chap. 7.

The observed linearity of the signal with respect to the weak signal field (Fig. 9.22) is in agreement with (9.5.3) and does not require separate discussion. Note that the proportionality m_z and h_s can be employed in order to measure the amplitudes of the weak microwave signals without registering, in the linear mode. Note also that according to (9.5.3) the measurements of the low-frequency oscillations amplitude m_z is a very sensitive method for obtaining stationary magnetization variation Δm_z, which is proportional to the number of parametrically excited magnons.

9.5.6 Other Methods for Excitation of Collective Oscillations

In Sec. 7.2.3 the theory of the direct excitation of collective oscillations by the longitudinal radio-frequency field at the frequency was worked out. *Orel* and *Starobinets* [9.48] experimentally observed this phenomenon. The detailed comparison of the theoretical and experimental data has been performed in Ref. [9.48] and we shall not dwell on it here. Note only that their experimental data on the dependence of χ'' on supercriticality at resonance are completely described by (7.2.16). The observed frequency of collective oscillations also qualitatively coincides with the frequency calculated from (9.5.1) as well as the experimental data of [9.46] obtained by the above-described method of excitation by a weak microwave signal. Therefore, the S-theory adequately describes the microwave and radio frequency resonance

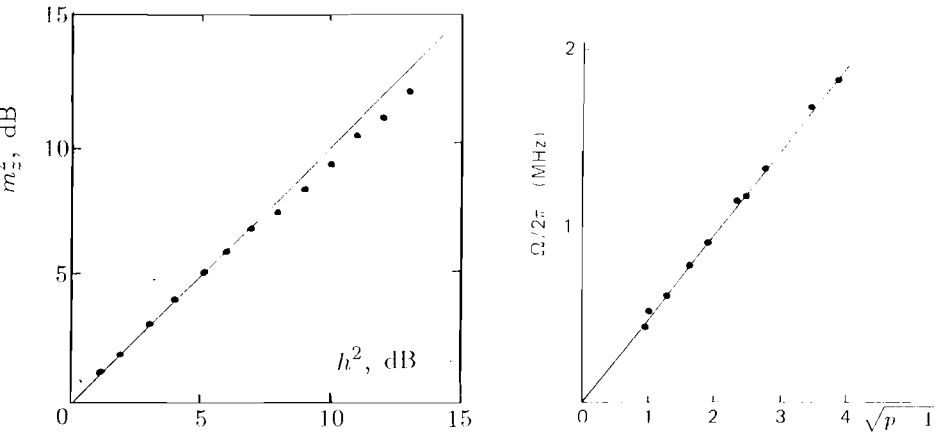

Fig. 9.22. (left) Power of low-frequency oscillations versus power of weak signal for YIG sphere at $\boldsymbol{M} \parallel [100]$, $H_c - H = 100$ Oe. After *Zautkin* et al. [9.46]

Fig. 9.23. (right) Resonant frequency of collective oscillation versus supercriticality for antiferromagnets $MnCO_3$ (*Prozorova* and *Smirnov* [9.46])

of collective oscillations, which agrees with the experimental data and requires no fitting parameters. This confirms the correctness of our physical concept of the nature of collective oscillations.

Closely related to the resonance methods of exciting collective oscillations is the method of excitation of collective oscillations by means of a drastic change in the pumping phase. This method was realized by *Prozorova* and *Smirnov* [9.36]. Their data on the natural frequency of collective oscillations in the antiferromagnet $MnCO_3$ are also in complete agreement with the theoretical dependence (9.5.1) (see Fig. 9.23).

9.6 Stepwise Excitation in YIG

As has been shown in Chap. 5, one of the main conclusions of the basic S-theory is the stage-by-stage excitation of wave packets that are singular in $\boldsymbol{k}$-space. This means that when the microwave power is increased smoothly, first a narrow packet is excited, for which h_{th} is minimum. When the power is increased further this packet is not broadened. Only when the microwave field reaches a strength h_2 exceeding h_{th} by 8 to 10 dB, is another group of waves created discontinuously. The observation of the influence of the size effect and of magnon-phonon peaks in the relation $h_{\text{th}}(\boldsymbol{H})$ shows that this conclusion is correct.

The simple distribution form of magnons at $h < h_2$ makes it possible to obtain analytical expressions for the most important characteristics of

the system of parametric magnons within the wide range of the pumping intensity. The good agreement between calculated and measured results for the susceptibility and collective resonance of parametric magnons (see Sec. 9.2, 3 and 5) indirectly confirm this conclusion. Special experiments are required for the direct proof of the excitation of waves with $\Theta = \pi/2$. They will be described below.

9.6.1 Re-Radiation into the Transverse Channel

Zautkin et al. [9.49] found a direct experimental proof of the stage-by-stage excitation. A YIG sample was put into a cylindrical resonator with two degenerate orthogonal modes (TE_{112}), whose magnetic fields $\boldsymbol{h}_\parallel$ and $\boldsymbol{h}_\perp$ were parallel and perpendicular, respectively, to the static field $\boldsymbol{H}$. The required polarization of the modes and their decoupling was achieved by the definite orientation of the waveguides connecting the resonator with the generator and input device.

The parallel channel ($\boldsymbol{h}_\parallel$) was used for the parametric excitation of magnon pairs with the frequency $\omega(\boldsymbol{k})/2\pi = 4.7$ GHz; the perpendicular channel ($\boldsymbol{h}_\perp$) registered the radiation of the sample at the pumping frequency $\omega_p = 2\omega(\boldsymbol{k})$. Up to the magnon excitation threshold, the decoupling between the channels was 55 dB. A drastic increase in radiation power was observed (see Fig. 9.24) in the perpendicular channel at a supercriticality $p_{cr} \simeq 8$–12 dB. (Different values of p_{cr} are due to the variations in the constant field, and the orientation and shape of the samples.) The radiation in the perpendicular channel is the result of the interaction of a magnon pair $a(\boldsymbol{k}), a(-\boldsymbol{k})$ with the uniform precession of the magnetization a_0 a which is described by the Hamiltonian

$$\mathcal{H}_\perp = \frac{1}{2}\sum_{\boldsymbol{k}}[u^*(\boldsymbol{k})a_0^* a(\boldsymbol{k})a(-\boldsymbol{k}) + \text{c.c.}]\,, \tag{9.6.1}$$

where $u(\boldsymbol{k}) = u\sin(2\Theta)\exp(i\Phi)$. The radiation power is determined by the expression

$$P_\perp = h_\perp^2 \simeq |\sum_{\boldsymbol{k}} u^*(\boldsymbol{k})a(\boldsymbol{k})a(-\boldsymbol{k})|^2\,, \tag{9.6.2}$$

which vanishes for $\Theta = 0$ and $\Theta = \pi/2$. The dependence $P_\perp(h_\parallel)$, plotted in Fig. 9.24 is a conclusive evidence of the fact that in the p range from 0 to 8 dB, only magnons pairs propagating at an angle $\Theta = \pi/2$ are excited. The radiation appearing at higher supercriticalities is naturally associated with the excitation of the second group of pairs with $\Theta \neq \pi/2$. The presence of the second threshold can also be observed by the characteristic distortion of the pumping pulse. A series of consecutive thresholds, first observed in this manner by *Petrakovsky* and *Berzhansky* [9.50] in YIG, is evidently associated with the stage-by-stage excitation of parametric magnons.

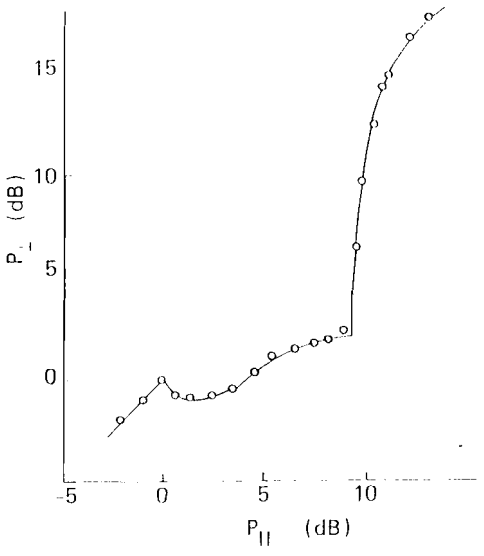

Fig. 9.24. Radiation power in transverse channel versus pumping power for YIG sphere at $\boldsymbol{M} \parallel [100]$, $H_c - H = 100$ Oe, $\omega_p/2\pi = 9.4$GHz. After *Zautkin* et al. [9.49]

9.6.2 Interaction of Second–Group Magnons and Transverse Signal

Methodologically, this experiment can be considered an "active" version of the above experiment. The main part of the setup is, as before, the bimodal cylindrical resonator TE_{112}. The mode $h_\parallel \equiv h_s$ is intended for parallel pumping of magnons, and the mode excited by the klystron is used for generation of an additional weak signal probing the system of parametric magnons. The interaction with the transversal weak signal is described (as in the previous case) by the Hamiltonian $\mathcal{H}_\perp$ (9.6.1) with the amplitude $u(\boldsymbol{k}) \simeq \sin 2\Theta$ and is allowed, therefore, only for the spin waves with $\Theta \neq \pi/2$. This interaction leads either to absorption or to amplification of the weak signal caused by the excitation of collective oscillations in the system of parametric magnons. In order to detect them we employ the sweeping of the klystron frequency by changing the voltage on its repeller plate with respect to the pumping frequency (coinciding with the frequency of the resonator). The signal with low combination frequency periodically changing within the range of 1 MHz excites the collective oscillations of magnons with $\Theta \neq \pi/2$. At the same time an additional peak of the weak signal absorption appears on the curve of the signal reflected from the resonator and having the shape of the resonance curve of the resonator.

The resonance peak of collective oscillations of the new group of parametric spin waves ($\Theta \neq \pi/2$) appears at a threshold h_{cr} as a weak distortion of the resonance curve in its center. As h increases and becomes higher and higher above the threshold of the interaction with the field of the transverse signal h_{cr} the peak becomes greater and is shifted from the central frequency.

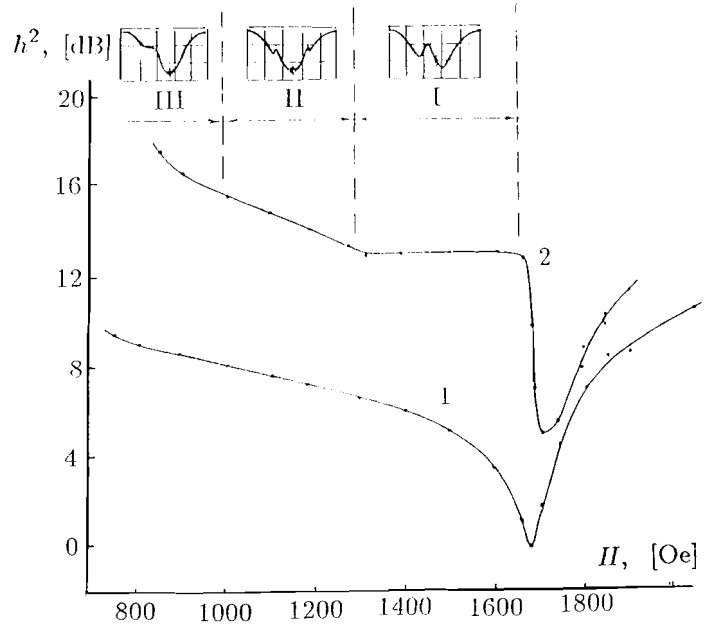

Fig. 9.25. Threshold of parametric excitation of magnons h^2_{th} (curve 1) and threshold of their interaction with transverse weak signal h^2_{cr} (curve 2) versus magnetic field for YIG sphere at $\boldsymbol{M} \parallel [100]$. After *Zautkin* et al. [9.51]

Figure 9.25 plots the experimental power dependences of the thresholds h_{th} and h_{cr} on the constant magnetizing field obtained by *Zautkin* [9.45] for the YIG sphere with the orientation $\boldsymbol{M} \parallel [100]$. The first threshold h_{th} was obtained with an accuracy of 0.1 dB from the distortion of the magnetron pulse reflected from the resonator. The threshold h_{cr} was registered with an accuracy of 0.5 dB from the distortion of the resonance curve on the oscillogram of the signal reflected from the resonator from the klystron side, i.e. using the above-described procedure.

The absence of the weak signal absorption at $h_{th} < h < h_{cr}$ over the entire range of the constant fields $H < H_c$ is the direct proof of the fact that below the threshold h_{cr} only the pairs with $\Theta = \pi/2$ are excited in the system (recall that H_c is the magnetic field under which $\omega_p = 2w(\boldsymbol{k})$ at $k = 0$ and $\Theta = \pi/2$). The values $h_{cr}/h_{th} \simeq 7$–12 dB (for different magnitudes of the field H) agree with the experimental data for re-irradiation into the transverse channel.

The phenomena observed in the range $H > H_c$ (Fig. 9.25) show that only the waves with $\Theta \neq \pi/2$ actually interact with the transverse weak signal. Indeed, at $H > H_c$ the bottom of the spin wave spectrum (the value $\omega(k, 0)$ at $k = 0$, $\Theta = \pi/2$) exceed $\omega_p/2$. It means that only the long wave part of the spectrum with some $\Theta < \Theta_* < \pi/2$ appears to be at the parametric resonance with the pumping. This removes the exclusion of the

magnon interaction with the field of the transverse channel and, as a result, collective oscillations induced by the field h_s emerge practically immediately above the first threshold and naturally there appears the absorption peak of the weak signal. The sharp decrease of the threshold of this effect after the passage through H_c leaves no doubt that the threshold is associated with the distribution change of parametric magnons in Θ.

For this reason the point on the curve $h_{cr}(H)$ at $H_c - H = 350$ Oe is of particular interest. The natural assumption of its association with the changed distribution of the registered parametric magnons is confirmed by the changed character of the interaction between the parametric magnons and the field of the weak signal reflected from the inserts in Fig 9.25 (for details see [9.51]). Fig. 9.26 plots the threshold of the interaction with the transverse weak signal h_{cr} versus the theoretical threshold values for the higher groups of parametric magnons as a function of the constant magnetic field. The comparison shows that in the fields $H_c - H \geq 300$ Oe the threshold of interaction with the field h_{cr} practically coincides with the calculated value of the second threshold of parametric magnons h_2, calculated in Sect. 6.1 (see also [9.51]). The discrepancy between them in the fields $H_c - H < 300$ Oe can be explained by the fact that the susceptibility of the second packet of parametric magnons to the transverse signal $\chi''(\omega_p + \Omega)$ is proportional to $u^2(\boldsymbol{k}) \sim \cos^2\Theta \sin^2\Theta$ (see (9.6.1)) and decreases as the magnetic field increases (see the points for the $\cos\Theta_2$ in Fig 9.26B). The calculation of the second packet susceptibility shows that for the fields $H_c > H > H_c - 300$ Oe and the pumping power $h^2 < 10h_{th}^2$ the magnitude of $\chi''(\omega_p + \Omega)$ is too small: $\chi'' \simeq 3 \cdot 10^{-3}$. Consequently, within this range of magnetic field values the distribution change in parametric magnons above the second threshold is not registered experimentally.

In this case the generation of the third group of parametric magnons at $h = h_3 > h_2$ is experimentally perceived as the "second threshold". In order to be able to interpret the experimental results, the threshold of generation of the third group of parametric magnons h_3 must be known, because h_{cr} must coincide with h_3.

This calculation of the threshold has been carried out by *Podivilov* [9.52] who widely used the theory of change in the distribution function of magnons above the intermediate threshold described in Sec. 6.1. His calculations of the thresholds and angles of generation of the third group of parametric magnons are shown in Fig. 9.26. In this figure the point of the third threshold calculated in [9.51] at $H_c - H = 100$ Oe when the second group emerges on the equator of the resonance surface leading only to the broadening of the parametric magnon packet with respect to the angle Θ is also shown.

The complete plot of the dependence $h_{cr}(H)$ in Fig 9.26 shows that in the fields $H < H_c - 300$ Oe the value h_{cr} corresponds to the excitation threshold of the second group of parametric magnons h_2 and for $H > H_c - 300$ Oe it

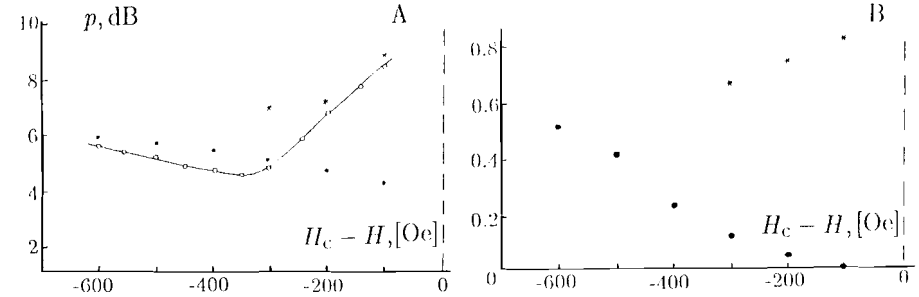

Fig. 9.26. Magnetic field dependence of the threshold of parametric excitation (Fig. A) and of the cosine of polar angles (Fig. B) in YIG sphere at $\boldsymbol{M} \parallel [100]$. Dots 1 are theory for a second group of pairs, dots 2 are theory for a third group p_3 and dots 3 are experimental data for the threshold of the parametric magnon interaction with weak signal. After *Zautkin* et al. [9.51, 52]

corresponds to the generation threshold of the third group h_3. In this case the salient point of the experimental curve discussed above can naturally be accounted for by the different field dependence of the threshold of the second and third groups of spin waves.

9.7 Conditions of Excitation of Auto-Oscillations of Magnons

As shown in Sec 8.1.3, the auto-oscillations under parametric excitation of waves are due to the instability of the ground state with respect to the variation of amplitudes and phases of the parametric waves, i.e, to the instability of the collective oscillations. When there is axial symmetry in the problem (e.g. under parallel pumping of magnons in cubic ferromagnets at $\boldsymbol{M} \parallel [100]$ or [111]) the criterion of generation of auto-oscillations according to this theory has the following form (7.1.1):

$$(S_m + S_{-m})(S_m + S_{-m} + 4T_m) < 0\,. \tag{9.7.1}$$

Here m is the number of the axial mode, S_m and T_m denote the axial Fourier harmonics of the interaction amplitudes of the waves. Values S_m and T_m in the cubic ferromagnets differ from zero at $|m| \leq 2$. (7.1.5) give the explicit expressions for these amplitudes through such parameters of the problem as the magnetization, pumping frequency, demagnetization factors (sample shape), etc. From these formulae and inequality (9.7.1) it is possible to predict the emergence of auto-oscillations in different experimental situations. Fig 9.27 shows the instability region of the mode $m = 0$ as a phase diagram on the plane $(\omega_p/\omega_m\ ,\ \ N_{z0,eff})$ [9.52]. The "instability phase" over which auto-oscillations take place is between the lines $S_0 = 0$ and

$2T_0 + S_0 = 0$, i.e. within the boundaries of the stability region of the mode $m = 0$. Putting aside the comparison with the experiment for the time being note some properties of the zero oscillation mode immediately following from Fig. 9.27. First, it is clear that as the ratio ω_p/ω_m increases, the instability region "broadens" with respect to $N_{z0,ef}$ and as $|N_{z0,ef}|$ decreases, it becomes wider with respect to ω_p/ω_m. For example, for crystallographic isotropic ($\omega_a = 0$) thin disc magnetized in the plane ($N_z = 0$) the instability occurs at any magnetization or pumping frequency. Another important peculiarity is a sharp asymmetry with respect to the sign change of the factor $N_{z0,ef}$: the negative values of $N_{z0,ef}$ correspond to the larger part (area) of the instability region. This accounts for the experimentally observed [9.28, 51] abnormally high crystallographic anisotropy of auto-oscillations in YIG. However, the well-known rule that auto-oscillations exist at the orientation $\boldsymbol{M} \parallel [111]$ and practically vanish at $\boldsymbol{M} \parallel [100]$ is not always observed, as can be seen from Fig. 9.27, it is also confirmed experimentally (see Table 9.2 below). This fact can now be easily explained: the parameter of the crystallographic anisotropy enters into the instability criterion (9.7.1) in a complex combination with other parameters (7.1.5) and the result is determined only by the relation of their numerical values.

Making use of the explicit form of the functions $S_{\pm 2}$ and $T_{\pm 2}$ (7.1.5) and of the criterion (9.7.1) we can also obtain the instability region of the modes $m = \pm 2$ (see Fig. 9.28). In comparison with the zero mode whose instability condition is independent of the magnitude of the wave vector k and parametric spin waves, modes $m = \pm 2$ are unstable only within some interval Δk corresponding to a certain region of positive values of $N_{z2,ef}$. Therefore, for $\boldsymbol{M} \parallel [100]$ (magnetization in the "difficult" direction, where the zero mode is often stable) the auto-oscillations of modes $m = \pm 2$ are usually arise.

The considered mode $m = 0$ and even modes $m = \pm 2$ (inhomogeneous in the azimuthal angle) are homogeneous in the sample volume, i.e. have a zero wave vector. Naturally, along with these modes, there can exist spatially inhomogeneous modes of auto-oscillations caused by the instability of some part of the spectrum of the collective oscillations propagating with the wave vector $\boldsymbol{\kappa} \neq 0$. Indeed, if the space dispersion is taken into account, to each mode of collective oscillations there corresponds a whole branch of the spectrum $\Omega_m(\kappa)$, whose gap $\Omega_m = \Omega_m(0)$ is given by (7.6.1). The spectrum of collective waves is described in Sec. 7.1.3. In the simplest case when $\boldsymbol{\kappa} \parallel \boldsymbol{M}$, $m = 0$ it is specified by (7.1.13):

$$\Omega_0(\kappa) = -i\gamma \pm \sqrt{[2(T_0 + S_0)N + \omega''\kappa^2/2]^2 - 4T_0^2N^2 - \gamma^2}\,, \qquad (9.7.2)$$

where $\omega'' = \partial^2\omega(k)/\partial k_z^2$. For the transverse perturbations ($\boldsymbol{\kappa} \perp \boldsymbol{M}$) the branches of oscillations with different m prove to be connected with each other and the normal modes appear to be their linear combinations. In this case a simple analytical expression cannot be written.

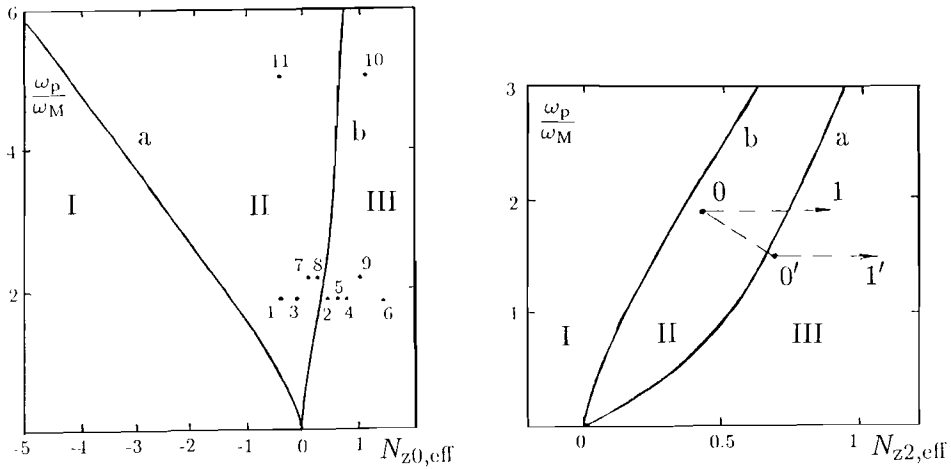

Fig. 9.27. (left) Theoretical stability phase diagram for collective mode m=0 in YIG. I and III are the regions of stability, II is the unstable region (intense auto-oscillations are predicted and observed). After *Zautkin* et al. [9.52]

Fig. 9.28. (right) Theoretical stability phase diagram for collective mode $m = \pm 2$ in YIG. I and III are the regions of stability, II is the unstable region (weak auto-oscillations are predicted and observed). After *Zautkin* et al. [9.52]

Figure 9.29 shows the possible variants of behavior $\Omega^2(\boldsymbol{\kappa})$ at $\gamma = 0$. The region of the negative values of Ω^2 corresponds to the instability of the ground state, which leads to the self-excitation of collective waves. Note that the ground state of the parametric wave system is always stable with respect to perturbations with large κ.

9.7.1 Experimental Setup

Auto-oscillations were investigated [9.52] for the system of parametric magnons excited by parallel pumping (see, for instance, setup in Fig. 9.1). The electromagnetic field with the frequency $\omega_p/2\pi = 9.37$ GHz was excited in the resonator by a magnetron with pulsed operation (pulse duration was 0.1–1 ms) or in a continuous mode. To avoid excessive sample heating in the continuous mode of operation the measurements were taken with an intensity not high above the threshold of parametric excitations. In addition the sample was cooled by compressed air. Samples of cubic ferromagnets with garnet structures were investigated with different magnetizations and anisotropic fields (see Table 9.1). The samples had a spherical shape 0.8–2.2 mm in diameter or were shaped as discs with the diameter of 4 mm and thickness of 0.1–0.2 mm. Magnetization orientation was selected along the most symmetrical directions, i.e. along the "easy" [111] and "difficult" [100] axes of the crystals.

Auto-oscillations of magnetization were registered by the amplitude modulation of the microwave field in which the sample was placed. The detected signal proportional to the reflection coefficient or to the passage coefficient was observed on the screen of the two-beam oscillograph. In the case of weak oscillations the pulse modulated by them had been pre-differentiated and amplified by a wide-band amplifier.

Along with the study of the properties of auto-oscillations the investigation of the induced oscillations near the instability limit was of fundamental interest. They were excited by the combination resonance between the pumping and the weak signal of similar frequency (this procedure has been described in Sec. 9.5). All the measurements were taken in the region of the magnetic fields $H < H_c$ corresponding to the excitation of the spin waves with $k \simeq 10^5$ cm^{-1}.

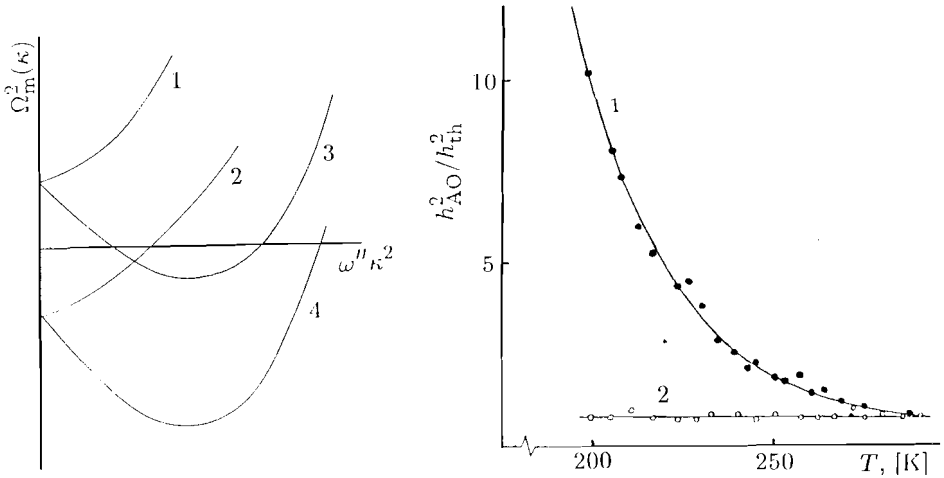

Fig. 9.29. (left) Examples for spectra of collective oscillations (9.7.2) (curves 1, and 2 correspond to condition $(T+S)\omega'' > 0$, curves 3 and 4 to $(T+S)\omega'' < 0$

Fig. 9.30. (right) Temperature dependences of auto-oscillation threshold in YIG sphere at $\boldsymbol{M} \parallel [100]$ (curve 1) and $\boldsymbol{M} \parallel [111]$ (curve 2). After *Zautkin* et al. [9.52]

9.7.2 Intensive Auto-Oscillations of Mode $m = 0$

In the early experiments by *Zautkin* et al. [9.52] auto-oscillations of comparatively large amplitude were investigated which could be observed directly as a low-frequency envelope of the microwave pumping pulse. As a whole, the picture of instability development observed in these experiments was qualitatively similar to those already known and described, e.g., in [9.28, 51, 52]. The attention was mainly paid to the validation of the instability criterion (9.71).

Table 9.2. Strong auto-oscillations (AO) in different cubic ferromagnets: YIG – $Y_3Fe_5O_{12}$ ($4\pi M$ =1750 Oe, H_a =84 Oe); YIScG – $Y_3Fe_{4.35}Sc_{0.65}O_{12}$ ($4\pi M$ =1500 Oe, H_a =8 Oe); ViCaIVG – $Vi_{0.2}Ca_{2.8}Fe_{3.6}V_{1.4}O_{12}$ ($4\pi M$ = 650 Oe, H_a =58 Oe) (After *Zautkin* and *Starobinets* [9.52], $\omega_p/2\pi = 9.8$ GHz, T= 300 K)

Crystal	Number of expt.	N_z	Direction of magnet.	Sign of $S_0(2T_0+S_0)$	Strong AO
YIG	1	0	[111]	–	present
	2	0	[100]	+	absent
	3	1/3	[111]	–	present
	4	1/3	[100]	+	absent
	5	1	[111]	+	absent
	6	1	[100]	+	absent
YIScG	7	0	[100]	–	present
	8	1/3	[100]	–	present
	9	1	[100]	+	absent
ViCaIVG	10	1/3	[100]	+	absent
	11	1/3	[111]	–	present

To this end, *Zautkin* and *Starobinets* [9.52] realized 11 different experimental situations and calculated from (7.1.5) the quantity $S_0(2T_0+S_0)$ for each of them. The results tabulated in Table 9.1 show that in all cases there is a complete agreement between the stability of the observed state of the parametric magnon system and the sign of the product $S_0(2T_0+S_0)$. The experimental situations in the table are in correspondence with the points on the state diagram of the homogeneous collective oscillations ($m = 0$) plotted in Fig. 9.27. Clearly, the intense oscillations are excited only when the corresponding point on the Fig. 9.27 is in the instability region of the zero mode. Therefore, the shape of the sample, its magnetization and its crystallographic anisotropy which determine the position of the point on the diagram can have a strong impact on the excitation of auto-oscillations of the system of parametric magnons. The diagram in Fig. 9.27 with experimental points is an attempt to systematize the data on auto-oscillations which proved to be successful owing to the introduction of the criterion (9.7.1). It must also be noted that if intense auto-oscillations exist, they are observed over the entire range of the magnetic field according to the fact

that the instability condition of the zero mode is independent of the value of the wave vector of spin waves.

9.7.3 Crossing the Instability Boundary and Spatially Inhomogeneous Auto-Oscillations

Let us compare theory with experiment on a more profound level. The points 2 and 8 on the phase diagram are of a special interest (Fig. 9.27). These points are close to the stability boundary ($2T_0 + S_0 = 0$) and at a slight change of temperature (increase for point 2 and decrease for point 8) they cross this boundary. Such transitions involving the state change have been experimentally observed. Fig. 9.30 shows the behavior of the excitation threshold of the intense auto-oscillations at the transition of point 8 (YIG with the addition of scandium at $\boldsymbol{M} \parallel [100]$) to the stability region accompanied by a temperature decrease. It turns out in this case that auto-oscillations do not disappear abruptly, their amplitude decreases smoothly as the transition to the stability region of the mode $m = 0$ proceeds.

In the second experiment (point 2 – disc-shaped YIG sample) auto-oscillations in the sample emerged at heating up to 360 K. The calculated value of the transition temperature obtained from the condition $2T_0 + S_0 = 0$ allowing for (7.1.5) is 330 K which is in satisfactory agreement with the experiment.

Such temperature transitions over the instability boundary $2T_0 + S_0 = 0$ enable us to verify the following statement. If the intense auto-oscillations are really the result of the instability of the zero mode of collective oscillations then at transition from the stable state into the unstable state the eigenfrequency $\Omega_0 = 2\sqrt{S_0(2T_0 + S_0)N}$ of the homogeneous mode must tend to zero. The check experiment [9.52] was based on the collective resonance of parametric magnons described in Sec. 9.5. It turned out that as the temperature increases the resonance feature of the absorption peak really decreases which is very important for the interpretation of the experiment, but does not tend to zero. In addition, near the critical temperature in the spectrum of the weak signal passage at the frequency $\omega_p + \Omega$ alongside with the dip there appears a peak of negative absorption at the image frequency $\omega_p - \Omega$ corresponding to the signal amplification.

The amplification of the weak signal is basically important from the viewpoint of the concept of collective resonance developed in Sec. 7.2. Let us turn to (7.2. 11) for the resonance susceptibility of the system of parametric spin waves in the field of the weak signal. The value of the radicand in it for the YIG is of the order of unity and therefore the absolute value of the negative susceptibility $\chi''(\omega_p - \Omega)$ is much less than the positive susceptibility $\chi''(\omega_p + \Omega)$. This can account for the absence of the amplification effect in experiments described in Sec. 9.5.3. However, in the cases when $S_0 \simeq 0$ or $2T_0 + S_0 \simeq 0$, the negative susceptibility according to (7.2.11) becomes in principle arbitrarily great which explains the possibility of the

electromagnetic radiation being amplified by the collective oscillations of parametric magnons close to the boundary of their instability. The opposite statement also holds true: the emergence of amplification indicates that the value $S_0(2T_0 + S_0)$ approximates zero. The fact that we do not experimentally observe a total vanishing of the resonance absorption frequency of the weak signal can be explained by Fig. 9.29. As can be seen from this figure, the continuous spectrum of collective oscillations always include such regions of the wave vectors $\boldsymbol{\kappa}$ for which instability appears earlier than for the homogeneous mode that can interact with the weak signal. For example, if for the branch 3 in Fig 9.29 the size of the gap decreases when the experimental conditions (temperature) are changed, then the inequality $\Omega_0^2 < 0$ is satisfied earlier for some $\kappa \neq 0$. The resulting auto-oscillations will be significantly spatially inhomogeneous; their amplitude obtained from the modulation depth of the pumping field depends on the "admixture" of the homogeneous mode which increases as it goes deeper into the instability region.

The spatial inhomogeneity of the auto-oscillations must also be manifested in the dependence of their frequency on the sample size d. Experimentally, it is observed as the increased frequency of the auto-oscillations when the sample size is decreased, but the frequency behavior cannot be described by a simple dependence proportional to $1/d$ and is significantly dependent on the length of the wave vector of spin waves.

Within the suggested model the frequencies of the collective oscillations (9.7.2) increase as the general number of magnons N becomes larger. In Fig. 9.29 it corresponds to the increased gap and the upward shift of the entire considered spectrum branch of the collective oscillations. Therefore, not far from the instability boundary the absence of the auto-oscillations can be reached by increasing the pumping intensity. This effect is really observed in the longitudinally magnetized YIG disc (point 2 in Fig. 9.27).

An interesting situation occurs when crossing the boundary $S_0 = 0$ (until now all the transitions referred to crossing the boundary $2T_0 + S_0 = 0$ on the phase diagram. At $S_0 \to 0$ the second threshold corresponding to the excitation of a new group of magnons with $\Theta \neq \pi/2$ tends to the first threshold (the self-consistent interaction of magnons limiting the energy flux from the pumping into the pairs with $\Theta \neq \pi/2$ disappears). The emergence of a new group of parametric magnons ordinarily is accompanied by the excitation of auto-oscillations. Therefore the auto-oscillations exist usually on the both sides of the boundary $S_0 = 0$. It makes impossible to observe experimentally crossing this boundary.

9.7.4 Instability of Higher Collective Modes

Now let us consider the auto-oscillations due to the instability of higher modes of collective oscillations with which $m \neq 0$ disturb the isotropic distribution of pairs in the azimuthal angle and therefore weakly interact with the homogeneous pumping field. Experiments carried out by *Zautkin* and *Starobinets* [9.52] on the setup with the improved sensitivity revealed the presence of weak auto-oscillations in some regions of magnetic fields. Earlier such auto-oscillations had been described in [9.28]. The authors of [9.52] choose a situation when the theory predicts stability for the mode $m = 0$ and instability for the modes $m = \pm 2$. This is the case of the YIG sphere at the orientation $\boldsymbol{M} \parallel [100]$. Fig. 9.31 shows the observed dependence of the threshold of weak auto-oscillations on the magnetic field in this case. It can be seen here that there are auto-oscillations in two regions of the fields. In the intermediate region auto-oscillations arise at the supercriticality 8 dB, but it is naturally associated with the generation of a new group of magnons above the second threshold and, consequently, has nothing in common with the modes $m = \pm 2$. Therefore these points are not shown on the plot. Auto-oscillations in the region I in Fig. 9.31 can be easily explained by the phase diagram depicting the instability region of the modes $m = \pm 2$ in Fig. 9.28. This diagram shows the trajectory of the point corresponding to the YIG sphere under the changed magnetic field. The initial point 0 corresponding to $k = 0$ (at $H = H_c$) is in the instability region. As the magnetic field H decreases, the wave number k, and, consequently, the coefficient $N_{z2,ef}$ increase (see (7.15)) and the point moving along the trajectory 01 comes out of the instability region. The theoretical width of the instability region found from condition (9.7) allowing for (7.1.5) for YIG at room temperature is equal to 550 Oe. The experimental value of the region 1 width in Fig 9.31 depending on the shape and size of the sample changes within the range 150–250 Oe.

As the temperature drops this region narrows, and region I vanishes completely at temperatures below 275 K. This is due to the increased anisotropy and magnetization leading to the shift of the initial point on the phase diagram along the line 00′ (see Fig. 9.28). Now it is clear that the trajectory 0′1′ corresponding to the change of field H at low temperatures does not cross the instability region of the modes $m = \pm 2$ at all.

The position of region II in Fig. 9.31 coincides with the field range where a hard excitation of parametric spin waves caused by the negative nonlinear damping [9.53] is observed. The auto-oscillations in this region are of a complex nature due to the interaction of the parametric and thermal spin waves with delayed reaction of the waves to the change in the state of the parametric subsystem. The generation of such auto-oscillations has been analyzed by *L'vov* in [9.54]. The peculiarity of these oscillations as distinct from the oscillations in region I is a continuous noise spectrum immediately

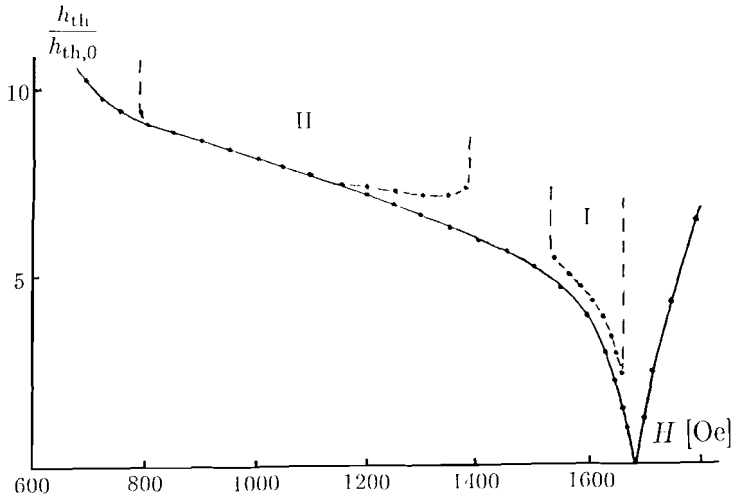

Fig. 9.31. Threshold of parametric excitation of magnons h_{th}^2 (solid curve) and threshold of weak auto-oscillations (dashed curve) versus magnetic field for YIG sphere at $\boldsymbol{M} \parallel [100]$. After *Zautkin* et al. [9.52]

above the threshold of the oscillations generation in a wide range of fields H coinciding with the threshold of parametric excitation.

In conclusion, we can say that the comparison of the theory of auto-oscillation generation under the parametric excitation of waves with a whole series of experiments on cubic ferromagnets described in Sec. 9.7 shows that the S-theory naturally gives an adequate quantitative description of various fine and often unexpected effects and *without making use of fitting parameters*. Among those effects are the influence of crystallographic anisotropy, temperature and shape of the sample on the properties of the auto-oscillations.

9.8 Effect of Radio-Frequency Field Modulation on Parametric Resonance

9.8.1 Suppression of Parametric Instability by Modulation

In Sec. 7.3 the influence of the periodic modulation of external magnetic field $\boldsymbol{H}(t)$ on the threshold of parametric excitation of magnons was studied theoretically. In order to verify the conclusions of this investigation, *Zautkin* and *Orel* [9.55] performed experiments on different types of modulation under parallel pumping of magnons in YIG at the frequency of 9370 MHz. The measurement procedure was standard, employing the pulsed operation with a pulse duration of 0.5 ms. The modulating field was produced by

generator current of rectangular, sinusoidal or saw-tooth pulse signals in the coil built in the resonator of the microwave pumping. Fig. 9.32 shows the threshold field of the parametric pumping versus the amplitude of modulation of different types. The initial sections of all curves are quadratic in H_m. At $H_m \gg 0.3$ Oe the transition to the mode of strong modulation takes place. The theory developed in Sec. 7.3 in this case predicts the excitation of two packets of spin waves with wave vectors $\boldsymbol{k}_1$ and $\boldsymbol{k}_2$ such that $\omega(\boldsymbol{k}_1) - \omega(\boldsymbol{k}_2) = 2U(k)H$. Because of the $\boldsymbol{k}$-dependence of the damping γ the thresholds of excitation of the packets $\boldsymbol{k}_1$ and $\boldsymbol{k}_2$ must be somewhat different. Indeed, at $H_m \geq 0.3$ Oe in a certain frequency region two successive thresholds are observed, of which the larger is manifested more sharply, i.e. the time of the instability development corresponding to it is much shorter.

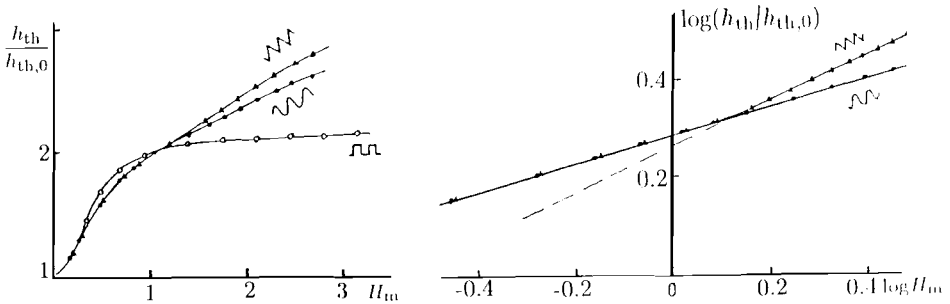

Fig. 9.32. (left) Threshold of parametric excitation of magnons h_{th}^2 versus amplitude of magnetic field modulation of different forms. Experiment in YIG sphere at $\boldsymbol{M} \parallel [100]$. $H_c - H = 100$ Oe, Modulation frequency $\Omega/2\pi = 0.3$ MHz. After *Zautkin* et al. [9.55]

Fig. 9.33. (right) Log-log plot for threshold of parametric excitation of magnons h_{th}^2 versus modulation frequency (saw-tooth and sinusoidal signals) Experiment in YIG sphere at $\boldsymbol{M} \parallel [100]$. $H_c - H = 100$ Oe, After *Zautkin* et al. [9.55]

In the mode of strong modulation the dependence $h_{th}(H_m)$ for the RF signal of rectangular shape in full agreement with the theory reaches the plateau when $h_{th}/h_{th,0} = 2$ is attained ($h_{th,0}$ – the threshold amplitude at $H_m = 0$). Two other modulation types lead to the monotonic increase of the threshold; at the same time the strongest influence at large H_m is exercised by the saw-tooth modulation. For the qualitative comparison of the obtained dependences with the theory it is convenient to approximate them by the functions $h_{th} \sim H_m$ for which the calculated values h_{th} (7.3.6, 7) yield the values $r = 2$ for the small amplitude of any shape, $r = 1/3$ for the sinusoid of large amplitude and $r = 1/2$ for the saw-tooth pulses. Fig. 9.33 shows the experimental curves in rectifying the logarithmic coordinates. Clearly, the dependences $h_{th}(H_m)$ are really adequately described by the power functions, the slopes of straight line segments correspond to

the exponents of power $r_{exp} = 2$ for small modulation amplitudes of any shape, $r_{exp} = 0.34$ for a strong sinusoidal modulation and $r_{exp} = 0.45$ for a strong saw-tooth modulation. Therefore, the ideas developed in Sec. 7.3 are experimentally verified. It must be noted, however, that as the modulation frequency changes, the numerical values of the parameters also change somewhat. In particular, the saturation of the threshold in the case of rectangular modulation takes place at $h_{th}/h_{th,0} = 1.8$–2.4 with the frequency variation being within the range $\Omega/2\pi = 0.2$–0.5 MHz. Evidently, this is due to the limited frequency region to which the approach of Sec. 7.3 can be applied assuming that the excited wave packet has no time for the shift in the k-space when the field $H_m(t)$ is changed.

9.8.2 Stationary State of Parametric Magnons Under Modulation of Their Frequency

This state has been treated theoretically in Sec. 7.4.1. From the obtained equations (7.4.3-5) we can find the nonlinear susceptibilities χ' and χ'' of the system of parametric magnons under the modulation of their frequency. This yields awkward expressions with the complex coefficients Γ and S (7.4.3,4). It is much more convenient to represent the p-dependences χ' and χ'' graphically for the given values of the amplitude and modulation frequency calculated on a computer. Figures 9.34A, 35A show the theoretical dependences of the susceptibility on the supercriticality of the pumping for $H_m = 0.15$ Oe, $\Omega/2\pi = 1.6$MHz and $\Omega_m/2\pi = 0.8$ MHz as well as the curves $\chi(p)$ obtained from the formulae of the basic S-theory (5.5.35) for the parallel pumping of magnons in YIG without the field modulation plotted here for the sake of comparison.

Figures 9.34B, 35B show the experimental dependences χ' and χ'' on the supercriticality for $H_m = 0$, $H_m = 0.15$ Oe and some values of Ω [9.56]. The experimental data were obtained like in Sec. 9.11 with the constant field being oriented along the axis [001] of the YIG crystal.

All the curves in Figs. 9.34, 35, theoretical as well as experimental, show that the reaction of parametric magnons to the modulating radio-frequency field has a resonance character. As can be expected the maximum deflections of the susceptibilities from their stationary values are near the resonance of collective oscillations when the supercriticality attains the value under which the eigenfrequency of these oscillations $\Omega_0(p)$ determined by it becomes equal to the modulation frequency Ω. Therefore as the frequency of the RF modulation increases, the maximum of the resonance change in susceptibilities shifts towards higher supercriticalities. Comparing the calculated dependences in Fig. 9.34 and 9.35 with the experimental values of the corresponding parameters of the RF signal (curve 3 in Fig 9.34B and curve 2 in Fig. 9.35B) we can see the same order of magnitude of the effect, i.e. RF addition to the susceptibility, effect sign at the resonance point and the characteristic change of sign at a distance from the resonance due to

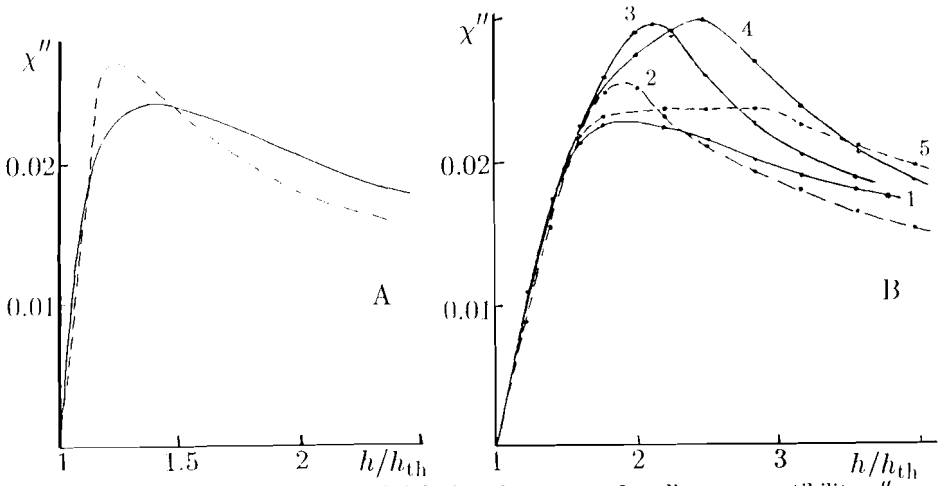

Fig. 9.34. Theory (A) and experiment (B) for imaginary part of nonlinear susceptibility χ'' versus pumping power for a YIG sphere ($H = H_c - 100$Oe, $\boldsymbol{M} \parallel [100]$) under modulation of the magnon frequency. Solid curve in (A) corresponds to $H_m = 0$, dashed line in (A) to H_m =0.14 Oe. Curves 1, 2, 3, 4 and 5 in (B) correspond to $\Omega/2\pi$ 0.0, 0.8, 1.2, 1.6, and 3.2 MHz. (H_m =0.14 Oe). After *Zautkin* et al. [9.56]

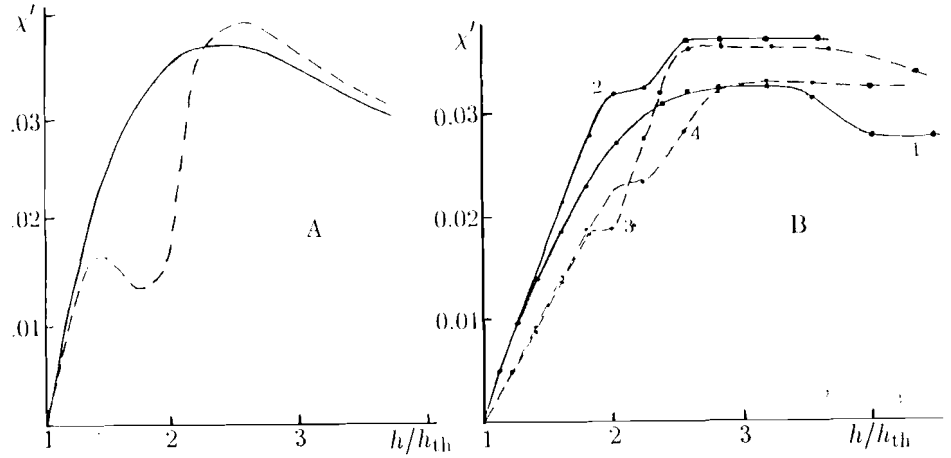

Fig. 9.35. Theory (A) and experiment (B) for real part of nonlinear susceptibility χ' versus pumping power for a YIG sphere ($H = H_c - 100$Oe, $\boldsymbol{M} \parallel [100]$) under modulation of the magnon frequency. Solid curve in (A) corresponds to $H_m = 0$, dashed line in (A) to H_m =0.14 Oe. Curves 1, 2, 3 and 4 in (B) correspond to $\Omega/2\pi$ 0.0, 0.8, 1.6 and 2.4 MHz. (H_m =0.14 Oe). After *Zautkin* et al. [9.56]

the supercriticality change. Therefore, we can conclude that the agreement of theory and experiment is satisfactory.

9.9 Double Parametric Resonance and Inhomogeneous Collective Oscillations of Magnons

Parametric excitation of collective oscillations in the system of parametrically excited waves – *double parametric resonance* was observed and experimentally studied by *Zautkin* et al. [9.56]. In their investigation three parallel magnetic fields were applied to a spherical sample of YIG, i.e. H – a constant magnetizing field; $h\exp(-i\omega_p t)$ – the microwave pumping; $H_m \exp(-i\Omega t)$ – RF pumping. The RF field was produced by a miniature coil located in the center of the microwave resonance. The measurements were taken in the RF range from 0.1 to 10 MHz. Parametric oscillations at the frequency $\Omega/2$ appeared at some critical value of the RF field. The signal at the frequency $\Omega/2$ induced in the coil was amplified by the selective receiver and registered on the oscillograph. The emergence of the signal had a threshold character. As H_m increased the signal almost disappeared in the threshold manner, i.e. its amplitude became 10 times smaller.

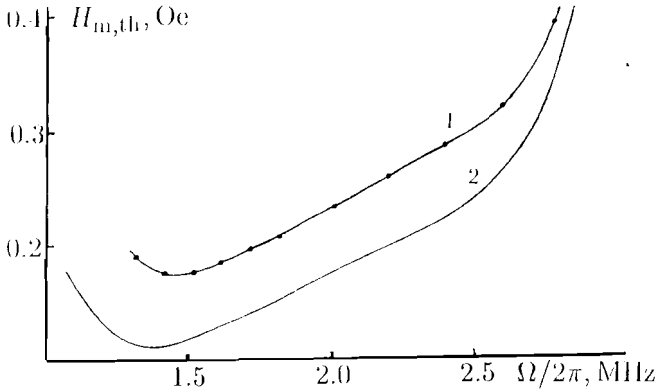

Fig. 9.36. Threshold of double parametric resonance $H_{m,th}$ versus modulation frequency $\Omega/2\pi$ in YIG sphere at $\boldsymbol{M} \parallel [100]$. $H_c - H = 100$ Oe. Curve 1 is experiment at $p = 2.5$ (4 dB), curve 2 – theory for Ω_0/γ=3.4 ($\gamma/2\pi$=0.37 MHz). After *Zautkin* et al. [9.46]

Figure 9.36 shows one of the experimental dependences $H_{m,th}(\Omega)$ (at $H = H_c - 100$ Oe, supercriticality equal to 4 dB) and the respective theoretical curve obtained from the condition of the zero determinant (7.4.10) (see also Fig. 7.1). The two curves are in good agreement with the exception, perhaps, of the low frequency region where the signal is very weak and no reliable measurements of the threshold can be performed. Note that the theory developed in the approximation quadratic in H_m predicts the existence of only one threshold $H_{m,th}$ under the fixed frequency Ω and supercriticality p. At the same time, in the experiment the second threshold is observed, i.e. the threshold of disappearance of collective oscillations as H

increases. Physically, this threshold is connected with the H_m dependence of the frequency of collective oscillations leading to the violation of the condition of parametric resonance. However, its actual calculation is difficult because higher-order terms in H_m must be allowed for $H_{m,th}(\varphi)$ and can be entirely impossible within the perturbation theory with respect to UH_m/γ.

In conclusion, note that we considered the spatially homogeneous collective oscillations with the wave vector $\kappa = 0$. Alongside in the system of parametric magnons there exists a wide spectrum of collective oscillations (see Fig. 9.29). Some intervals of this spectrum in principle can be parametrically excited by a homogeneous RF field at the frequency satisfying the condition $\Omega = \Omega(\kappa) + \Omega(-\kappa)$. These oscillations with $\kappa = 0$ have no stable connection with the resonator and consequently the radiation at the half-frequency will be significantly weakened. *Zautkin* and *Orel* [9.57] managed not only to register the fact of the existence of inhomogeneous collective oscillations at the double parametric resonance but also to investigate the spectrum. They employed a series of indirect data and analyzed experimentally obtained dependences of the frequency and amplitude of collective oscillations on H, H_m and h.

9.10 Parametric Excitation of Magnons Under Noise Modulation of their Frequencies

9.10.1 Threshold Amplitude of Noise Pumping

In Sec. 6.7 we described the nonlinear theory of the parametric excitation of waves by the noise pumping $h(t) = h(t)\exp(-i\omega_p t)$. Experimentally (see [9.58]) it proved to be more convenient to modulate the frequency of magnons by the longitudinal magnetic field $H_m(t)$. Employing the Hamiltonian (4.3.19) we can easily see that

$$\omega(\boldsymbol{k}, t) = \omega(\boldsymbol{k}) + H_m(t)U(\boldsymbol{k}) \,, \tag{9.10.1}$$

Here $U(\boldsymbol{k})$ is the interaction amplitude of the longitudinal field $H_m(t)$ with magnons. Using the canonical equations of motion (5.2.2) with the frequency (9.10.1), and after the substitution of variables

$$b(\boldsymbol{k}, t) = c(\boldsymbol{k}, t)\exp[-i\varphi(t)], \quad \varphi(t) = U(\boldsymbol{k})\int_{-\infty}^{t} H_m(\tau)d\tau \,, \tag{9.10.2}$$

one has the equations with constant frequency and the pumping

$$h(t) = h\exp[-2i\varphi(t)] \,. \tag{9.10.3}$$

Therefore, the modulation of the magnon frequency (9.10.1) really proves to be equivalent to the modulation of the pumping phase (9.10.3).

The experiment by *Zautkin* et al. [9.58] was performed on the YIG crystals under parallel pumping at the frequency of 9.37 GHz. The experimental setup includes a rectangular resonator and ordinary waveguide elements connected in a circuit "for reflection". The pulsed operation of the magnetron with a pulse frequency of 25 Hz and a duration of 0.6 ms was employed. The threshold of parametric excitation of spin waves and their susceptibility were determined by the procedure described in Sec. 9.1.1, i.e. by the change of signal reflected from the resonator. For the noise modulation of the field through the coil built in the resonator a current from the noise generator was transmitted through a set of filters of lower frequencies and a wide-band amplifier. The generator produces a noise signal with a constant spectral density in the range Δf = 0–7 MHz. Such a noise can be considered "white" since its band significantly exceeds the relaxation frequency $\gamma/2\pi \simeq 0.4$ MHz and other characteristic frequencies, as will be shown below. Such conditions are most interesting from the viewpoint of the concept developed in Sec. 6.7. The filters reducing the frequency band of the noise signal provide for the determination of the influence of the problem parameters on the process of parametric excitations.

Figure 9.37 shows the experimental dependences of the threshold amplitude (on the coordinates $h_{th}^2/h_{th,0}^2$) on the spectral density of the noise field $H_m^2(0)$. For the rectangular shape of the spectrum $H_m^2(\Omega)$ with the width Δ (in the linear frequency) $H_m^2(0) = \langle H_m^2\rangle/2\Delta$; $\langle H_m^2\rangle$ is the mean square value of $H_m(t)$. First it must be noted that as Δ increases, the modulation influence on the threshold field becomes stronger (see curves 1,2 and 3 for Δ = 0.8, 2.0 and 4.0 MHz). Then this dependence is saturated and curves 3 and 4 for Δ = 4.0 and 8.0 MHz coincide. Apparently, the noise modulation at $\Delta < 3$ MHz is not "sufficiently white".

Compare curves 3 and 4 with the theoretical dependence (6.7.1) of the threshold field

$$h_{th}^2 V^2 = \gamma(\gamma + \Delta) \,, \tag{9.10.4}$$

which is accurate if the phase fluctuations of the pumping field $h(t)$ (i.e. the process $H(t)$ are the white Gaussian noise. In (9.10.4) Δ is the correlator of phase fluctuations, i.e.

$$\langle\varphi(t)\varphi(t')\rangle = \Delta\delta(t - t') \,. \tag{9.10.5}$$

Allowing for (9.10.2) the threshold formula (9.10.4) can be rewritten as

$$[h^2/h_{th,0}^2 - 1] = U^2 H_m^2/\gamma \,. \tag{9.10.6}$$

Here $h_{th,0}^2 = \gamma^2/V^2$ is the threshold power at $H_m = 0$. Clearly, in full agreement with the theoretical dependence (9.10.6) lines 3 and 4 in Fig. 9.37 are straight. According to (9.10.6) the tangent of the slope $k = U^2/\gamma$. For the yttrium garnet under experimental conditions $U = 2{\cdot}10^7$ sec$^{-1}{\cdot}$Oe^{-1}

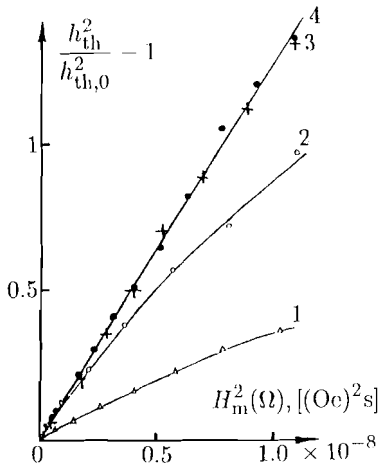

Fig. 9.37. Experimental dependences of the threshold of parametric excitation of magnons h^2_{th} on the spectral power of noise $H^2_m(0)$ for YIG sphere at $M \parallel [100]$, $H_c - H = 100$ Oe. Curves 1, 2, 3 and 4 correspond to spectral widths Δ equal to 0.8, 2.0, 4.0 and 8.0 MHz. After *Zautkin* et al. [9.58]

and for the slope of the straight line at the value $2\gamma = 2\pi \cdot 0.75 \cdot 10^6$ sec^{-1} we obtain the value $K = 1.7 \cdot 10^8$ sec$^{-1} \cdot$ Oe^{-2}. The experimental data (see Fig. 9.37) are $K_{exp} = (1.3 \pm 0.3) \cdot 10^8$ sec$^{-1} \cdot$ Oe^{-2}. Despite a large error in obtaining K_{exp} due to the large error of the modulation coil calibration we must emphasize the qualitative agreement of the theoretical value K_{theor} and experimental results.

9.10.2 Efficiency of Phase Mechanism Under Noise Pumping

The most important characteristics of the above-threshold state of the system of parametric magnons from the viewpoint of the S-theory are the total number N and the phase shift Ψ of the pair with respect to the pumping phase. Therefore, most significant in the investigation of the nonlinear behavior of magnons above the threshold is the measurement of the complex susceptibility whose imaginary part χ'' characterizes its total number N and the real part χ' essentially depends on the phase relations in the system.

Zautkin et al. [9.58] measured χ'' and χ' by a standard method (see Sec. 9.1.1), their experimental setup is shown in Figs. 9.1. Figures 9.38, 39 show their experimental dependences of the susceptibilities χ' and χ'' on the supercriticality at different spectral densities of the noise field H_m for the largest band of the noise frequencies $\Delta f = 7$ MHz. For the set of the given dependences it is characteristic that not high above the threshold the noise significantly reduces the susceptibility χ'', and at greater p it somewhat increases it. As a result, with increasing H the whole curve χ'' is shifted towards large p, its shape remaining similar to the respective curves for the coherent pumping (curve 1 in Fig 9.38). The behavior of the real part of the susceptibility χ' is similar: noise influence is strongest near the threshold, at the same time χ' is significantly reduced, but as

the pumping intensity increases, its difference from the susceptibility in the coherent mode decreases. At the maximum point the difference is less than 30%. Note that even at the highest value of the spectral density of the noise the maximum value of χ' (Fig. 9.39) exceeds χ'' for the same value of H_m.

Even without a quantitative comparison of the advanced S-theory conclusions with the noise pumping considered in Sec. 6.7 (it will be performed later) we can assert that the above results point to the presence of phase correlations in the system of parametric spin waves and in the case of the noise pumping. The main evidence of the effect of the phase mechanism of the amplitude limitation is that $\chi' \neq 0$. Other mechanisms, as already mentioned, are purely dissipative and result in a zero real susceptibility. In the experiment [9.58] χ' is not only non-zero, but is essentially not small, it exceeds the imaginary part of χ'' similarly to the case of coherent pumping. In addition, the significant similarity of the behavior of $\chi'(p)$ and $\chi''(p)$ with the respective dependences obtained in the absence of noise reveals that the mechanism limiting the parametric magnon increase in this case is the same.

In order to compare theory with experiment in more detail, the nonlinear susceptibilities χ', χ'' must be calculated under noise pumping. Employing the ideas developed in Sec. 5.5.5, 6.7, *Cherepanov* [9.58] got

$$\chi'' = \chi_m \begin{cases} (p-1)^{3/2}/3\sqrt{3}p & \text{at } (p-1) \ll 1 \\ 3\sqrt{3}\sqrt{p-1}/16p & \text{at } p \gg 1 \end{cases} \tag{9.10.7}$$

$$\chi' = \chi_m \begin{cases} 2(p-1) & \text{at } p-1 \ll 1 \\ 1 & \text{at } p \gg 1 \end{cases} \tag{9.10.8}$$

Here $\chi_m = 2V^2/|S|$. For comparison, we represent the nonlinear susceptibilities under coherent pumping (5.5.35) in the same notation

$$\chi'' = \chi_m \sqrt{p-1}/p\,, \quad \chi' = \chi_m(p-1)/p\,. \tag{9.10.9}$$

For the sake of convenience of the comparison of theory with experiment, Fig. 9.40 shows also the experimental values of the quantity $\chi''p$ proportional to the absorbed power as a function of $p-1$. The graph is plotted in the logarithmic coordinates where (9.10.7, 8) specify the linear relation of these values. The singularities of the noise pumping expressed in the finite formulae of the theory (9.10.7, 8) are clearly seen on the resulting diagram. The diagram has two rectangular sections, the tangent of its slope at small $p-1$ being equal to 1.4 which agrees with the exponent of power equal to 1.5 in (9.10.7). At large p the slope coincides with the slope of the respective straight line for the coherent pumping depicted for better comparison with the same coordinates in Fig. 9.40. Equation (9.10.7) for χ''(p) also coincides (up to the constant factor) with χ''(p) for coherent pumping (9.10.9).

Now let us compare the numerical values of the measured susceptibilities with their calculated values. Equation (9.10.7) for the imaginary part of the

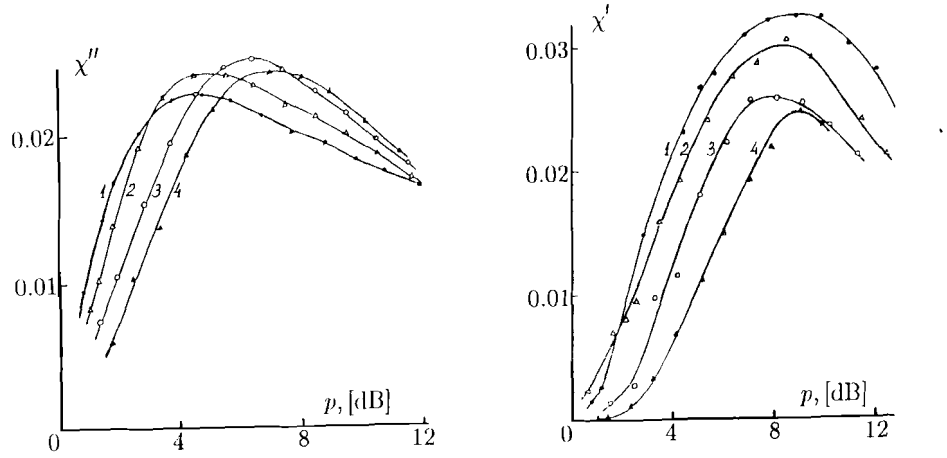

Fig. 9.38. (left) Experimental dependences of the imaginary part of the nonlinear susceptibility χ'' on the pumping power p under noise modulation in YIG sphere at $\boldsymbol{M} \parallel [100]$, $H_c - H = 100$ Oe. Curves 1, 2, 3 and 4 correspond to $H_m^2(0)$ equal to 0.0, $1.7 \cdot 10^{-9}$, $3.4 \cdot 10^{-9}$ and $5.1 \cdot 10^{-9}$ $(\text{Oe})^2 \cdot \text{s}$. After *Zautkin* et al. [9.58]

Fig. 9.39. (right) Experimental dependences of the real part of the nonlinear susceptibility χ' on pumping power p under the same experimental conditions as at Fig. 9.38

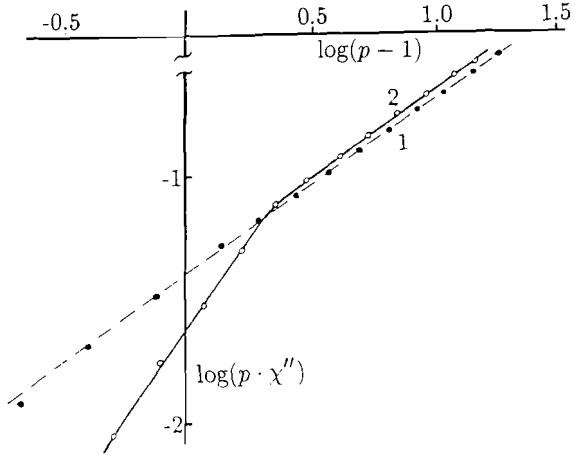

Fig. 9.40. Experimental dependences of the imaginary part of the absorption power $\propto \chi'' \cdot p$ on the pumping power $p - 1$ (in the log–log plot) under noisy modulation in YIG sphere at $\boldsymbol{M} \parallel [100]$, $H_c - H = 100$ Oe. Curves 1 and 2 correspond to $H_m^2(0)$ equal to 0.0 and $5.1 \cdot 10^{-9}$, $(\text{Oe})^2 \cdot \text{s}$. After *Zautkin* et al. [9.58]

susceptibility is in good agreement with the experimental data for the region of small supercriticalities. For instance, for $p = 2$ dB it follows from this formulae that $(\chi''/\chi''_m)_{\text{theor}} = (4/3\sqrt{3})(p-1)^{3/2} = 0.4446$, at the same time the experimentally obtained relation is $(\chi''/\chi''_m)_{\text{exp}} = 0.44(\pm 7\%)$. In the region of large supercriticalities there is a considerable discrepancy with (9.10.8), which yields $(\chi''/\chi''_m)_{\text{exp}} = 0.324$, at the same time $(\chi''/\chi''_m)_{\text{theor}} = 0.8$. As for the real part of the susceptibility, under high pumping intensity $(\chi')/\chi'_m)_{\text{theor}} = 1$ and $(\chi')/\chi'_m)_{\text{exp}} = 0.7$; such an agreement can be considered satisfactory. In the region of small supercriticalities there is a significant discrepancy at $p = 2$ dB we have $(\chi')/\chi'_m)_{\text{theor}} = (2/3)(p-1) = 0.48$, although $(\chi')/\chi'_m)_{\text{exp}} = 0.1$. These discrepancies are apparently caused by the fact that in the experiment the value $\Delta_{\text{ef}}/\gamma \simeq |h_{\text{th}} V^2|/\gamma^2$, was not sufficiently large (< 3), and at the same time expressions (9.10, 7, 8) had been obtained on the assumption that $\Delta_{\text{ef}}/\gamma \gg 1$,. Nevertheless, the agreement of the basic functional dependences (9.10.7,8) with the experimental results shows that the excitation level of parametric magnons under noise excitation is limited, as in the case of coherent excitation, by the mechanism of the phase detuning from the pumping, and our theory correctly describes their general behavior above the threshold.